

Evolution of large-amplitude Alfvén waves and generation of switchbacks in the expanding solar wind

ALFRED MALLET,¹ JONATHAN SQUIRE,² BENJAMIN D. G. CHANDRAN,³ TREVOR BOWEN,¹ AND STUART D. BALE^{1,4}

¹*Space Sciences Laboratory, University of California, Berkeley CA 94720, USA*

²*Physics Department, University of Otago, Dunedin 9010, New Zealand*

³*Space Science Center, University of New Hampshire, Durham, NH 03824, USA*

⁴*Physics Department, University of California, Berkeley CA 94720, USA*

(Dated: April 20, 2021)

ABSTRACT

Motivated by recent Parker Solar Probe (PSP) observations of “switchbacks” (abrupt, large-amplitude reversals in the radial magnetic field, which exhibit Alfvénic correlations) we examine the dynamics of large-amplitude Alfvén waves in the expanding solar wind. We develop an analytic model which makes several predictions: switchbacks should preferentially occur in regions where the solar wind plasma has undergone a greater expansion, the switchback fraction at radii comparable to PSP should be an increasing function of radius, and switchbacks should have their gradients preferentially perpendicular to the mean magnetic field direction. The expansion of the plasma generates small compressive components as part of the wave’s nonlinear evolution: these are maximized when the normalized fluctuation amplitude is comparable to $\sin \theta$, where θ is the angle between the propagation direction and the mean magnetic field. These compressive components steepen the primary Alfvénic waveform, keeping the solution in a state of nearly constant magnetic field strength as its normalized amplitude $\delta B/B$ grows due to expansion. The small fluctuations in the magnetic-field-strength are minimized at a particular θ -dependent value of β , usually of order unity, and the density and magnetic-field-strength fluctuations can be correlated or anticorrelated depending on β and θ . Example solutions of our dynamical equation are presented; some do indeed form magnetic-field reversals. Our predictions appear to match some previously unexplained phenomena in observations and numerical simulations, providing evidence that the observed switchbacks result from the nonlinear evolution of the initially small-amplitude Alfvén waves already known to be present at the coronal base.

1. INTRODUCTION

Alfvén waves are ubiquitous in the solar wind and corona (Belcher & Davis 1971), and are considered to be the basic building blocks of the turbulence that heats the corona and accelerates the solar wind. As the solar wind plasma travels away from the sun and expands, Alfvén waves carried along with the plasma decay in amplitude (Parker 1965). Flux conservation means that the overall (mean) radial magnetic field strength \bar{B}_R has a somewhat faster decay than the fluctuations: the combination of these two laws mean that the *normalized* amplitude of Alfvén waves, $\delta B/\bar{B}_R$, increases as the solar wind plasma travels away from the sun. Even

when the nonlinear effects of turbulence are taken into account (Cranmer & Van Ballegooijen 2005; Verdini & Velli 2007; Van Ballegooijen & Asgari-Targhi 2016; van Ballegooijen & Asgari-Targhi 2017; Perez & Chandran 2013; Chandran & Perez 2019), initially low-amplitude waves eventually attain a large normalized amplitude. In this paper, we study the dynamical evolution of Alfvén waves of arbitrary amplitude in the expanding solar wind.

Additional motivation for the study of large-amplitude Alfvén waves comes from the striking observation of “switchbacks”: large-amplitude, abrupt reversals of the magnetic field, observed by NASA’s Parker Solar Probe (PSP) mission in the inner solar wind and corona (Bale et al. 2019; Horbury et al. 2020; de Wit et al. 2020; Krasnoselskikh et al. 2020; Farrell et al. 2020; McManus et al. 2020; Mozer et al. 2020; Laker et al. 2020). These observations have prompted several attempts at theoretical

explanation, with different theories suggesting that they may be the result of coronal reconnection forming either flux ropes (Drake et al. 2020) or complex fast-mode-like structures (Zank et al. 2020), the nonlinear Kelvin-Helmholtz instability (Ruffolo et al. 2020), or differential flow between different solar wind sources (Schwadron & McComas 2021). An alternative, potentially much simpler hypothesis is that switchbacks may form naturally *in situ* from initially low-amplitude Alfvén waves (AWs) (Squire et al. 2020) due to the growth of their amplitude relative to the mean magnetic field in the expanding Solar Wind (Grappin & Velli 1996). These Alfvén waves are known to be ubiquitous in the corona already (De Pontieu et al. 2007; Van Ballegooijen & Asgari-Targhi 2016), and so if it works, this model does not require any “special event” to create the switchbacks.

Let us separate the magnetic field and velocity into their mean and fluctuations, $\mathbf{B} = \overline{\mathbf{B}} + \delta\mathbf{B}$, $\mathbf{u} = \overline{\mathbf{u}} + \delta\mathbf{u}$. In a homogeneous medium (constant mean velocity $\overline{\mathbf{u}}$ and magnetic field $\overline{\mathbf{B}}$), any configuration of magnetic field and velocity fluctuations with an Alfvénic correlation between its velocity and magnetic field fluctuations,

$$\delta\mathbf{u} = \pm\delta\mathbf{B}/\sqrt{4\pi\rho}, \quad (1)$$

which additionally has constant magnetic-field strength, density, and pressure,

$$B^2 = \text{const.}, \quad (2)$$

$$\rho = \text{const.}, \quad (3)$$

$$P = \text{const.}, \quad (4)$$

is an exact nonlinear solution to the MHD equations (Goldstein et al. 1974), propagating with group velocity equal to

$$\mathbf{v}_g = \pm\mathbf{v}_A = \pm\overline{\mathbf{B}}/\sqrt{4\pi\rho}, \quad (5)$$

the Alfvén velocity (in the frame in which $\overline{\mathbf{u}} = 0$), regardless of its amplitude; i.e. without steepening. This property is unique amongst the large-amplitude MHD waves. The properties (1–5) comprise the definition of a large-amplitude Alfvén wave in a homogeneous medium; we will also refer to this as a *perfect Alfvén wave*, and/or say that a configuration is *Alfvénic* if it satisfies (or nearly satisfies) (1–4). More often in the literature, only (1) is used to define the Alfvénic state, but the others are also necessary for a configuration to propagate at \mathbf{v}_A , and are crucial for large-amplitude waves. Due to (2), the magnetic-field vector moves on the surface of a sphere; thus, this configuration is also referred to as a “spherically-polarized Alfvén wave”. Moreover, (2) implies that, unlike the linearized Alfvén wave, the large-amplitude Alfvén wave has a parallel (to $\overline{\mathbf{B}}$) component δB_{\parallel} . This constraint also means that a monochro-

matic wave is impossible, since (2) involves both terms quadratic and linear in the fluctuations (Barnes & Hollweg 1974, see also Sec. 3.2).

Rather strikingly, all of (1–5) are (usually) nearly satisfied by many switchbacks (Bale et al. 2019; Kasper et al. 2019; Horbury et al. 2020)¹. This provides some simple but powerful evidence in support of the *in situ* Alfvén wave generation hypothesis: the Squire et al. (2020) model is currently the only one that naturally includes these basic correlations. Other models must invoke some (largely unspecified) process of “Alfvénization” (Drake et al. 2020; Ruffolo et al. 2020; Schwadron & McComas 2021) to explain the constant-magnetic-field-strength observation. Moreover, Squire et al. (2020) performed numerical simulations of expanding Alfvénic turbulence, and showed that the initial condition of random, small-amplitude, outward-propagating Alfvén waves, upon expansion, does indeed naturally produce switchbacks. Shoda et al. (2021) also found this using compressible MHD simulations in a narrow magnetic flux tube extending from the coronal base out to $40R_{\odot}$.

In an inhomogeneous medium, it can be shown that the overall root-mean-square (RMS) amplitude of a large-amplitude Alfvén wave obeys the same law as in the small-amplitude case (Hollweg 1974; Barnes & Hollweg 1974, see also Sec. 3.1). However, because $B^2 = (\delta\mathbf{B} + \overline{\mathbf{B}})^2$, and $\delta B/\overline{B}$ grows with expansion, small variations in B^2 are constantly being produced, and thus the expansion constantly pushes the wave out of its perfect constant- B^2 state. How is it then possible to maintain the Alfvénic nature of the wave over long timescales? In other words, while other models of switchback formation have problems explaining why the switchbacks *become* Alfvénic, an important question to ask of the Squire et al. (2020) Alfvén wave expansion model is how the switchbacks *remain* so Alfvénic, given the apparently harmful effects of expansion; this is the focus of the current paper. We attack the problem in a simplified fashion: we neglect every effect except a simple spherical expansion, and adopt the (locally-isothermal) Expanding Box MHD model (Velli et al. 1992; Grappin et al. 1993, henceforth EBM). We apply a two-timescale analysis (the details of which are in the next section) to arbitrary-amplitude Alfvénic fluctuations that, at any instant in time, vary along a single spatial direction. We show that the waveform of

¹ Recent evidence suggests, however, that there is a small but systematic variation in the compressive components (2–4) (Farrell et al. 2020; Larosa et al. 2020), a point to which we will return later.

Table 1. Predictions of the model, their location in the paper, and either existing observational evidence or a suggested observational test to confirm or falsify the model.

Prediction	Section	Observational evidence / <i>possible test</i>
Nearly-constant magnetic field strength (cf. Barnes & Hollweg 1974).	2	Agrees with Horbury et al. (2020) (among many others).
Larger amplitude with more expansion. (cf. Hollweg 1974)	3.1	<i>Switchbacks should occur in “patches” where the plasma has undergone more expansion (Bale 2021).</i>
Increasing switchback fraction with radial distance from the Sun.	3.1	Agrees with Mozer et al. (2020); Badman et al. (2020).
Angle-dependent threshold for radial field reversals: preference for perpendicular structures.	3.2	Agrees with Laker et al. (2020): switchbacks elongated along \bar{B} . Agrees with initial-condition dependence of switchback fraction in simulations (Squire et al. 2020).
Compressive components: scaling with expansion rate.	3.3	<i>Measure compressions as a function of expansion rate (cf. slow/fast wind as high/low expansion surrogates).</i>
Magnetic compressibility minimized for $\beta \sim 1$.	3.4	Agrees with simulations of turbulence (Squire et al. 2020).
Angle-dependent transition in polarization state $\xi = (\delta B /\bar{B})/(\delta\rho/\bar{\rho})$.	3.5	<i>Could be compared with Larosa et al. (2020).</i>

the primary Alfvénic component obeys a relatively simple dynamical equation (Eq. 59) on the slow expansion timescale. Physically, the expansion drives a small non-constant component of the magnetic pressure B^2 , which then drives a compressive flow, distorting the waveform.

The utility of our dynamical equation, introduced in Section 2, is that it allows us to make a number of detailed predictions that go beyond the basic properties of large-amplitude Alfvén waves (1–5); these are described in Section 3. We re-derive Hollweg’s 1974 result on the scaling of the amplitude of large-amplitude Alfvén waves with expansion, and thus predict that switchbacks should occur preferentially in patches of solar wind where the super-radial expansion of field lines and plasma is large (Sec. 3.1). We also argue that this amplitude evolution means that at radial distances R comparable to the perihelia of PSP, the fraction of the volume filled with fluctuations that reverse the radial field should be an increasing function of R , agreeing with the observations of Mozer et al. (2020) and Badman et al. (2020). Using a simple geometrical argument, we also show that it is easier for fluctuations to reverse the mean magnetic field and form switchbacks when the direction of variation (wavevectors) is nearly perpendicular to \bar{B} (Sec. 3.2) – this may partly explain the observations of Laker et al. (2020) that switchbacks are highly elongated along the mean magnetic field direction. A similar anisotropy of the switchbacks was observed in the numerical turbulence simulations of Squire et al. (2020), who also observed that the switchback fraction was significantly higher in runs for which there were more extremely perpendicular modes in the initial con-

dition². We outline the scaling properties of the new expansion-driven compressible components of the wave, and discuss how this is related to nonlinear steepening and distortion (Sec. 3.3). In Sec. 3.4, we show that the small variation in magnetic-field strength introduced by expansion is minimized at $\beta \sim 1$, which agrees with the turbulence simulations of Squire et al. (2020). Sec. 3.5 shows further that whether the small variations in B^2 and ρ are correlated or anti-correlated (“fast-wave-like” or “slow-wave-like” respectively) depends on the propagation angle and β , potentially explaining the fact that both these behaviours are seen in the observational data (Larosa et al. 2020). For clarity, all of these predictions are summarized in Table 1.

Having studied the general properties of our equation in some detail, we then present in Section 4 some sample numerical solutions of our dynamical equation with different initial conditions, examining the conditions which generically give rise to switchbacks and confirming the results of our scaling analyses.

2. DERIVATION OF THE SWITCHBACK EQUATION

In this Section, we will derive an equation governing the evolution of the waveform of an Alfvénic structure of arbitrary amplitude as it travels away from the Sun and expands. If the reader prefers to skip the details, a summary of our results is given in Sec. 2.6. Before we begin, we will briefly outline the major assumptions and restrictions of our analysis.

² In particular, their Gaussian initial conditions had more power in modes with large k_{\perp} initially.

First, our calculation uses the Expanding Box model (EBM, Velli et al. 1992; Grappin et al. 1993), which expresses the MHD equations in a small parcel of plasma, in a frame comoving with the mean solar wind velocity U (a constant in the EBM), undergoing spherical expansion (in the y - and z -directions) as it moves radially (in the x -direction) away from the sun. While constant U and spherical expansion are undoubtedly rather poor approximations to the corona, this model contains the important physical mechanism we are interested in: expansion makes $\overline{\mathbf{B}}$ and $\delta\mathbf{B}$ decay differently, thus increasing the normalized amplitude and also pushing the wave out of perfectly constant B^2 . Thus, we feel that the EBM is an acceptable minimal model with which to study the dynamics of large-amplitude Alfvén waves as they travel away from the sun. Moreover, the way it replaces all of the inhomogeneity in space with a time-dependent background (in the Expanding Box frame) will prove analytically very useful. In our analysis, we assume that the timescale of the Alfvénic fluctuations, T_A , is much shorter than the timescale associated with the expansion, T_{exp} . We then define the small parameter

$$\epsilon = \frac{T_A}{T_{\text{exp}}}, \quad (6)$$

and expand the solution to the EBM equations in powers of ϵ . We restrict ourselves to solutions for which the leading-order solutions for B^2 , ρ , and P are constant (cf. Eqs. 2–4). We additionally assume that in the initial condition, the solution varies only along a single spatial direction: the expansion of the box subsequently causes that direction to rotate with time, but at each instant, the solution is one-dimensional. We will repeat these major assumptions at the points at which each is introduced in the derivation.

As mentioned in the introduction, our assumption that B^2 , ρ , and P are constant to leading order is rather well motivated by the observational evidence, and means that our solutions behave at zeroth order like large-amplitude Alfvén waves. In addition, the smallness of ϵ does appear to be somewhat satisfied for the real switchbacks: Laker et al. (2020) found that the parallel length of the switchback is around $1R_\odot$, meaning their Alfvén time is $T_A \sim R_\odot/v_A$, while the expansion time around the radial location at which they are observed is $T_{\text{exp}} \sim 30R_\odot/V_{\text{SW}}$; using $v_A \approx 100\text{kms}^{-1}$ and $V_{\text{SW}} \approx 300\text{kms}^{-1}$, the ratio of these times is indeed a small parameter, $\epsilon \approx 1/10$. Our assumption of one-dimensional spatial variation, however, is more seriously objectionable: real switchbacks are clearly three-dimensional. This assumption limits the validity of our

solution to regions where the direction of the gradients is very close to constant.

Finally, let us point out two aspects of the solution that we do not restrict: we allow the zeroth order fluctuations of magnetic field and velocity to have arbitrary amplitude, and we permit any zeroth-order waveform for which B^2 is spatially constant.

2.1. Preliminaries

The starting point for our analysis is, as previously mentioned, the Expanding Box Model (EBM) (Velli et al. 1992; Grappin et al. 1993), which consists of the following equations:

$$\frac{\partial \rho}{\partial t} + \nabla \cdot (\rho \mathbf{u}) = -2\frac{\dot{a}}{a}\rho, \quad (7)$$

$$\frac{\partial \mathbf{u}}{\partial t} + \mathbf{u} \cdot \nabla \mathbf{u} = -\frac{1}{\rho} \nabla \left(c_s^2 \rho + \frac{B^2}{8\pi} \right) + \frac{\mathbf{B} \cdot \nabla \mathbf{B}}{4\pi\rho} - \frac{\dot{a}}{a} \mathbb{T} \cdot \mathbf{u}, \quad (8)$$

$$\frac{\partial \mathbf{B}}{\partial t} + \mathbf{u} \cdot \nabla \mathbf{B} = \mathbf{B} \cdot \nabla \mathbf{u} - \mathbf{B} \nabla \cdot \mathbf{u} - \frac{\dot{a}}{a} \mathbb{L} \cdot \mathbf{B}, \quad (9)$$

$$\nabla \cdot \mathbf{B} = 0, \quad (10)$$

where $\mathbb{T} = \text{diag}(0, 1, 1)$, $\mathbb{L} = \text{diag}(2, 1, 1)$, and $\nabla = (\partial_x, a^{-1}\partial_y, a^{-1}\partial_z)$. The co-moving coordinates $\mathbf{r} = (x, y, z)$ do not change as the plasma travels away from the sun and expands; the corresponding coordinates in the inertial, non-expanding frame moving with the solar wind velocity (a.k.a. the ‘‘solar wind frame’’) are $\mathbf{r}_g = (x_g, y_g, z_g) = (x, ay, az)$. The expansion factor $a = 1 + \dot{a}t$, and \dot{a} is a constant (because the solar wind velocity U is assumed constant); the expansion timescale $T_{\text{exp}} = a/\dot{a}$ (cf. Eq. 6). We assume that the plasma is locally isothermal, $c_s^2 = c_s^2(t)$. In the present analysis we will not need to specify the precise time dependence; part of our solution will be a function of the instantaneous value of $\beta = c_s^2/v_A^2$. We restrict ourselves to one-dimensional solutions that depend on the EBM spatial coordinates $\mathbf{r} = (x, y, z)$ only through the function

$$\lambda = \mathbf{p}^* \cdot \mathbf{r}, \quad (11)$$

where \mathbf{p}^* is constant in space and time; since the EBM coordinates are also constant in time, λ is not a function of t . In the inertial solar wind frame, these solutions vary along the time-dependent vector \mathbf{p} , written in terms of \mathbf{p}^* as

$$\mathbf{p}(t) = \nabla \lambda = \begin{pmatrix} p_x^* \\ p_y^*/a \\ p_z^*/a \end{pmatrix}. \quad (12)$$

We additionally assume (Eq. 6) that fluctuations vary on both a short timescale T_A and the long timescale

$T_{\text{exp}} = a/\dot{a}$, and take $\epsilon = \dot{a}T_A/a$ to be a small parameter. Specifically, we assume that a fluctuation f can be written in the form

$$f = f(\lambda, t, \tau), \quad (13)$$

where

$$\tau = \epsilon t. \quad (14)$$

We will use the notation

$$f_\lambda = \left. \frac{\partial f}{\partial \lambda} \right|_{t,\tau}, \quad f_t = \left. \frac{\partial f}{\partial t} \right|_{\lambda,\tau}, \quad f_\tau = \left. \frac{\partial f}{\partial \tau} \right|_{\lambda,t}, \quad (15)$$

to denote partial derivatives with respect to each of the arguments. In this one-dimensional case, the gradient of any function f may be written

$$\nabla f = \mathbf{p} f_\lambda, \quad (16)$$

We may write the partial time derivative at constant \mathbf{r} as

$$\begin{aligned} \left. \frac{\partial f}{\partial t} \right|_{\mathbf{r}} &= f_t + \frac{d\tau}{dt} f_\tau, \\ &= f_t + \epsilon f_\tau. \end{aligned} \quad (17)$$

We will additionally define

$$\alpha = \frac{\dot{a}}{\epsilon a}. \quad (18)$$

We proceed by separating all variables into their spatial mean and fluctuating components, e.g.

$$f = \bar{f} + \tilde{f}, \quad (19)$$

where

$$\bar{f}(t, \tau) = \frac{1}{\Lambda} \int_0^\Lambda f(\lambda, t, \tau) d\lambda, \quad (20)$$

and we require that the solution is periodic in λ with period Λ .³ Note that the spatial mean of the fluctuating component vanishes by definition, $\bar{\tilde{f}} = 0$.

We expand the fluctuations as follows:

$$\tilde{\mathbf{B}} = \mathbf{B}_0 + \epsilon \mathbf{B}_1 + \dots, \quad (21)$$

$$\tilde{\mathbf{u}} = \mathbf{u}_0 + \epsilon \mathbf{u}_1 + \dots, \quad (22)$$

$$\tilde{\rho} = \epsilon \rho_1 + \dots, \quad (23)$$

³ It is also possible to choose as the boundary condition that all quantities $f \rightarrow \bar{f}$ as $\lambda \rightarrow \infty$; since it is more numerically convenient, we use periodic boundary conditions in the present analysis. When comparing our results to the real world, it is important to remember that the EBM is only valid if $\Lambda \ll pR$.

where

$$\begin{aligned} B_0 &\sim B_1 \sim \dots \sim B_n \sim \bar{B}, \\ u_0 &\sim u_1 \sim \dots \sim u_n \sim v_A, \\ \rho_1 &\sim \rho_2 \sim \dots \sim \rho_n \sim \bar{\rho}, \end{aligned} \quad (24)$$

i.e., the amplitude of the zeroth-order fluctuation in \mathbf{B} , B_0 , is comparable to \bar{B} . Because we would like to study Alfvén waves, $\rho_0 = 0$ and so $\bar{\rho} \ll \bar{\rho}$. Similarly, we require the fluctuations in the magnetic field *strength* to be small:

$$\frac{\widetilde{B^2}}{B_0^2} \sim O(\epsilon). \quad (25)$$

Since, to first order,

$$B^2 = |\bar{\mathbf{B}} + \mathbf{B}_0 + \mathbf{B}_1|^2 = |\bar{\mathbf{B}} + \mathbf{B}_0|^2 + 2\epsilon(\bar{\mathbf{B}} + \mathbf{B}_0) \cdot \mathbf{B}_1, \quad (26)$$

we must therefore have

$$(\bar{\mathbf{B}} + \mathbf{B}_0) \cdot \mathbf{B}_{0\lambda} = 0. \quad (27)$$

Eq. (10) may be written

$$\mathbf{p} \cdot \mathbf{B}_\lambda = 0, \quad (28)$$

which upon integration over λ at constant t, τ means that

$$\mathbf{p} \cdot \mathbf{B} = g(t, \tau). \quad (29)$$

Taking the spatial mean of this equation, we find that $g(t, \tau) = \mathbf{p} \cdot \bar{\mathbf{B}}$, i.e.,

$$\mathbf{p} \cdot \mathbf{B} = \mathbf{p} \cdot \bar{\mathbf{B}}, \quad \mathbf{p} \cdot \tilde{\mathbf{B}} = 0. \quad (30)$$

2.2. Zeroth order

At this order, the expansion terms in (7–9) are absent since $\dot{a}/a \sim O(\epsilon)$, and the system reduces to the standard (one-dimensional) MHD equations. Writing this system in conservative form and taking the spatial mean, we find that, at zeroth order,

$$\bar{\rho}_t = 0, \quad \bar{\mathbf{u}}_t = 0, \quad \bar{\mathbf{B}}_t = 0, \quad (31)$$

and so at this order, our analysis recovers the properties of large-amplitude Alfvén waves in a constant, homogeneous background (Barnes & Hollweg 1974). We take $\bar{\mathbf{u}} = 0$; this is clearly consistent with these zeroth-order equations, and we will check later that this is also the case at first order.

Now, we subtract (31) from the relevant zeroth-order equations to find the fluctuating parts. The fluctuating part of the continuity equation (7) at zeroth order reads

$$\bar{\rho} \mathbf{p} \cdot \mathbf{u}_{0\lambda} = 0, \quad (32)$$

and so we may take $\mathbf{p} \cdot \mathbf{u}_0 = 0$ (using the same reasoning as led from Eq. 28 to Eq. 30). The fluctuating parts of the zeroth-order momentum (8) and induction (9) equations yield

$$\mathbf{u}_{0t} = \frac{\mathbf{p} \cdot \overline{\mathbf{B}}}{4\pi\bar{\rho}} \mathbf{B}_{0\lambda}, \quad (33)$$

$$\mathbf{B}_{0t} = \mathbf{p} \cdot \overline{\mathbf{B}} \mathbf{u}_{0\lambda}, \quad (34)$$

whose solutions are

$$\mathbf{u}_0 = \mathbf{u}_0(\lambda \mp \mathbf{p} \cdot \mathbf{v}_A t, \tau) = \mp \frac{v_A}{B} \mathbf{B}_0(\lambda \mp \mathbf{p} \cdot \mathbf{v}_A t, \tau), \quad (35)$$

where the constant of integration is zero because these are fluctuations. This solution propagates at group velocity $\pm \mathbf{v}_A$ in the inertial solar wind frame, and the relationship between the velocity and magnetic-field fluctuations is Alfvénic; it is an Alfvén wave, as expected. We will choose the lower sign in Eq. (35), and introduce Alfvén units for the magnetic field fluctuations,

$$\mathbf{b}_0 = \frac{\mathbf{B}_0}{\sqrt{4\pi\bar{\rho}}} = \mathbf{u}_0. \quad (36)$$

Finally, the zeroth-order solution shows that the Alfvén-wave timescale is $T_A \sim (\mathbf{p} \cdot \mathbf{v}_A)^{-1}$; for concreteness, we define

$$T_A = (\mathbf{p} \cdot \mathbf{v}_A)^{-1}. \quad (37)$$

2.3. First order

To go further, we will look for a solution in which all fluctuating quantities depend on λ and t only via $\lambda + \mathbf{p} \cdot \mathbf{v}_A t$ (as well as on τ); i.e., a (slowly-evolving) wave. This also means that we may express the t -derivative in terms of the λ -derivative,

$$f_t = \mathbf{p} \cdot \mathbf{v}_A f_\lambda, \quad (38)$$

thus removing the fast time dependence from the equations.

At first order, the mean of the continuity equation gives

$$\bar{\rho}_\tau + 2\alpha\bar{\rho} = -\overline{(\rho_1 \mathbf{u}_0)_\lambda}, \quad (39)$$

where we have used the fact that the spatial mean of a fluctuation is zero. The term on the RHS vanishes since it is the mean of a total derivative; thus,

$$\bar{\rho} \propto a^{-2}. \quad (40)$$

The fluctuating part of the continuity equation now gives

$$\mathbf{p} \cdot \mathbf{v}_A \rho_{1\lambda} + \bar{\rho} \mathbf{p} \cdot \mathbf{u}_{1\lambda} = 0, \quad (41)$$

and so

$$\boxed{\frac{\rho_1}{\bar{\rho}} = -\frac{\mathbf{p} \cdot \mathbf{u}_1}{\mathbf{p} \cdot \mathbf{v}_A}}, \quad (42)$$

using the fact that fluctuations have zero spatial average. The mean momentum equation at first order gives

$$\overline{\mathbf{u}_\tau} + \alpha \mathbb{T} \cdot \overline{\mathbf{u}} = -\overline{\mathbf{p}(\mathbf{b}_1 \cdot \mathbf{b}_0)_\lambda} - \overline{\mathbf{p} \cdot \mathbf{u}_1 \mathbf{u}_{0\lambda}} - \frac{\bar{\rho}_1}{\bar{\rho}} \overline{\mathbf{p} \cdot \mathbf{v}_A \mathbf{b}_{0\lambda}}. \quad (43)$$

The first term on the RHS results from the average of the total-pressure-gradient term; since it is the mean of a total derivative, it is zero. Upon inserting (42) and the zeroth-order solution (35), the second and third terms on the RHS cancel; thus $\overline{u_x} \propto a^0$, $\overline{u_{y,z}} \propto a^{-1}$, and if $\overline{\mathbf{u}} = 0$ initially, it will remain zero throughout the evolution. This shows that our assertion that $\overline{\mathbf{u}} = 0$ is also consistent at first order.

The fluctuating momentum equation at first order is

$$\mathbf{u}_{0\tau} + \mathbf{p} \left[c_s^2 \frac{\rho_1}{\bar{\rho}} + \mathbf{b}_1 \cdot (\mathbf{v}_A + \mathbf{b}_0) \right]_\lambda + \alpha \mathbb{T} \cdot \mathbf{u}_0 = \mathbf{p} \cdot \mathbf{v}_A (\mathbf{b}_1 - \mathbf{u}_1)_\lambda, \quad (44)$$

where we have used (42) to cancel some terms.

To analyse the induction equation, notice the following relation between the τ -derivative of \mathbf{B} and $\mathbf{b} = \mathbf{B}/\sqrt{4\pi\bar{\rho}}$:

$$\mathbf{b}_\tau = \frac{\mathbf{B}_\tau}{\sqrt{4\pi\bar{\rho}}} - \frac{\mathbf{b}\bar{\rho}_\tau}{2\bar{\rho}} = \frac{\mathbf{B}_\tau}{\sqrt{4\pi\bar{\rho}}} + \alpha \mathbf{b}. \quad (45)$$

Using this, the mean of the induction equation at first order is

$$\mathbf{v}_{A\tau} + \alpha \hat{\mathbf{x}} v_{Ax} = -\overline{\mathbf{p} \cdot \mathbf{u}_1 \mathbf{b}_{0\lambda}} - \overline{\mathbf{b}_0 \mathbf{p} \cdot \mathbf{u}_{1\lambda}}. \quad (46)$$

The terms on the RHS together comprise the mean of a total derivative, and are therefore equal to zero; thus,

$$v_{Ax} \propto a^{-1}, v_{Ay,z} \propto a^0. \quad (47)$$

Using (12) and (47), $\mathbf{p} \cdot \mathbf{v}_A = T_A^{-1} \propto a^{-1}$. It then follows from (6), (18) and (37) that

$$\epsilon = \frac{T_A}{T_{\text{exp}}} = \frac{\dot{a}}{a \mathbf{p} \cdot \mathbf{v}_A} = \text{const.}, \quad \frac{\alpha}{\mathbf{p} \cdot \mathbf{v}_A} = 1. \quad (48)$$

This relation will be useful in analysing the scaling properties of our solution in Sec. 3. The fluctuating induction equation at first order is

$$\mathbf{b}_{0\tau} + [\mathbf{p} \cdot \mathbf{u}_1 (\mathbf{v}_A + \mathbf{b}_0)]_\lambda + \alpha \hat{\mathbf{x}} \mathbf{b}_{0x} = \mathbf{p} \cdot \mathbf{v}_A (\mathbf{u}_1 - \mathbf{b}_1)_\lambda. \quad (49)$$

Inserting the zeroth-order solution $\mathbf{u}_0 = \mathbf{b}_0$ and taking the sum of (44) and (49), the RHS cancels, and we are left with

$$2\mathbf{b}_{0\tau} + [\mathbf{p} \cdot \mathbf{u}_1 (\mathbf{v}_A + \mathbf{b}_0)]_\lambda + \mathbf{p} \left[c_s^2 \frac{\rho_1}{\bar{\rho}} + \mathbf{b}_1 \cdot (\mathbf{v}_A + \mathbf{b}_0) \right]_\lambda + \alpha \mathbf{b}_0 = 0. \quad (50)$$

Taking the dot-product of this equation with \mathbf{p} gives a relationship between the first-order compressive fluctuations and the radial component of the zeroth-order magnetic-field fluctuation,

$$\left[c_s^2 \frac{\rho_1}{\rho} + \mathbf{b}_1 \cdot (\mathbf{v}_A + \mathbf{b}_0) \right]_\lambda = \frac{2\alpha p_x b_{0x}}{p^2} - \frac{(\mathbf{p} \cdot \mathbf{u}_{1\lambda})(\mathbf{p} \cdot \mathbf{v}_A)}{p^2}, \quad (51)$$

where we have used

$$\mathbf{p} \cdot \mathbf{b}_{0\tau} = (\mathbf{p} \cdot \mathbf{b}_0)_\tau - \mathbf{b}_0 \cdot \mathbf{p}_\tau = -\frac{\dot{a}}{a} p_x b_{0x}, \quad (52)$$

using Eq. (30) to express this in terms of b_{0x} only. This allows us replace the total-pressure gradient term in (50), giving

$$\mathbf{b}_{0\tau} + \frac{\alpha}{2} \left(\mathbf{b}_0 + \frac{2\mathbf{p}p_x}{p^2} b_{0x} \right) + \frac{1}{2} [\mathbf{p} \cdot \mathbf{u}_1 (\mathbf{v}_{AT} + \mathbf{b}_0)]_\lambda = 0, \quad (53)$$

where $\mathbf{v}_{AT} = \mathbf{v}_A - \mathbf{p}(\mathbf{p} \cdot \mathbf{v}_A)$ are the components of \mathbf{v}_A transverse to \mathbf{p} . This equation encodes the slow evolution of an arbitrary-amplitude Alfvén wave in the expanding solar wind. However, this evolution is not yet determined; to proceed, we need to write the compressive component $\mathbf{p} \cdot \mathbf{u}_1$ in terms of \mathbf{b}_0 .

2.4. Finding $\mathbf{p} \cdot \mathbf{u}_1$

Equation (53) comprises two independent equations for three unknowns (the two transverse components of \mathbf{b}_0 and $\mathbf{p} \cdot \mathbf{u}_1$); so we need one more equation to determine the evolution. This turns out to be provided by the condition (27) that the zeroth-order magnetic field strength is spatially uniform. Let us work in terms of the total zeroth-order magnetic field $\mathbf{b} = \mathbf{v}_A + \mathbf{b}_0$. Taking the partial derivative of $\mathbf{b}(\lambda, t, \tau)$ with respect to τ

$$[\mathbf{b}_1 \cdot (\mathbf{v}_A + \mathbf{b}_0)]_\lambda = \frac{2\alpha}{p^2} \left[p_x b_{0x} + \mathbf{p} \cdot \mathbf{v}_A \left(1 - \frac{\beta}{\cos^2 \theta} \right) \frac{b_{0x} (v_{Ax} + p_x \mathbf{p} \cdot \mathbf{v}_A / p^2) - \frac{1}{2} \mathbf{b}_0 \cdot \mathbf{v}_A}{|\mathbf{v}_{AT} + \mathbf{b}_0|^2} \right], \quad (58)$$

where θ is the angle between \mathbf{p} and \mathbf{v}_A . This equation describes how expansion creates a perturbation in the magnetic pressure.

⁴ Combined, of course, with a suitable initial condition at $\tau = 0$, and the appropriate periodic boundary condition in λ .

at constant λ and t , we obtain

$$\mathbf{b}_\tau = \mathbf{b}_{0\tau} - \alpha \hat{\mathbf{x}} v_{Ax}. \quad (54)$$

Inserting this into (53) and taking the dot product with \mathbf{b} , we obtain

$$\frac{1}{2} (b^2)_\tau + \alpha \left[b_x v_{Ax} + \frac{p_x \mathbf{p} \cdot \mathbf{v}_A}{p^2} b_{0x} + \frac{1}{2} \mathbf{b}_0 \cdot \mathbf{b} \right] + \frac{1}{2} \mathbf{p} \cdot \mathbf{u}_{1\lambda} |\mathbf{v}_{AT} + \mathbf{b}_0|^2 = 0, \quad (55)$$

where $|\mathbf{v}_{AT} + \mathbf{b}_0|$, the zeroth-order transverse magnetic field strength, is spatially constant (because $\mathbf{p} \cdot \mathbf{b} = \mathbf{p} \cdot \mathbf{v}_A$ is too, cf. Eq. 10). We now take the fluctuating part of this equation by subtracting its spatial mean; using the identity

$$\widetilde{\mathbf{b}_0 \cdot \mathbf{b}} = \widetilde{\mathbf{b} \cdot \mathbf{b}} - \widetilde{\mathbf{v}_A \cdot \mathbf{b}} = \widetilde{b^2} - \widetilde{v_A^2} - \mathbf{b}_0 \cdot \mathbf{v}_A, \quad (56)$$

(the first two crossed-out terms on the RHS are zero because both b^2 and \mathbf{v}_A are spatial constants) we are left with

$$\mathbf{p} \cdot \mathbf{u}_{1\lambda} = -2\alpha \frac{b_{0x} (v_{Ax} + p_x \mathbf{p} \cdot \mathbf{v}_A / p^2) - \frac{1}{2} \mathbf{b}_0 \cdot \mathbf{v}_A}{|\mathbf{v}_{AT} + \mathbf{b}_0|^2}, \quad (57)$$

an equation for the divergence of the first-order velocity in terms of \mathbf{b}_0 . Equations (53) and (57) determine the evolution of \mathbf{b}_0 on the expansion timescale,⁴ and are the main result of this paper.

2.5. Magnetic pressure fluctuations

As stated in Eq. (25), the magnetic pressure is constant at zeroth order. At first order, the gradient of the magnetic pressure is (in Alfvén units) $\epsilon \mathbf{p} [\mathbf{b}_1 \cdot (\mathbf{v}_A + \mathbf{b}_0)]_\lambda$. Using (42), (51) and (57), we may write this solely in terms of \mathbf{b}_0 ,

2.6. Physical summary

We will now briefly summarise our results before analysing their consequences in the next section. We collect the important equations (those which are boxed where they appear in the derivation) here for clarity. Our main result is a dynamical equation (53) governing the slow nonlinear evolution of an arbitrary-amplitude

Alfvénic fluctuation \mathbf{b}_0 as it travels out in the expanding plasma of the solar wind:

$$\mathbf{b}_{0\tau} + \frac{\alpha}{2} \left(\mathbf{b}_0 + \frac{2\mathbf{p}p_x}{p^2} b_{0x} \right) + \frac{1}{2} [\mathbf{p} \cdot \mathbf{u}_1(\mathbf{v}_{AT} + \mathbf{b}_0)]_\lambda = 0. \quad (59)$$

The τ -derivative term is the time derivative on the slow expansion timescale. The $\alpha\mathbf{b}_0/2$ term gives rise to the slow decay of the wave amplitude on the expansion timescale (see Sec. 3.1). The term in the \mathbf{p} -direction encodes the divergence-free nature of the magnetic fluctuations as the direction of the gradients, \mathbf{p} , rotates towards radial due to expansion. The final term is nonlinear, and describes the distortion of the primary Alfvénic fluctuation as it increases in normalized amplitude, by a compressive velocity

$$u_{1\text{comp}} = \epsilon \mathbf{p} \cdot \mathbf{u}_1 / p. \quad (60)$$

The gradient of this velocity is also determined as part of our analysis, in Eq. (57), which reads

$$\mathbf{p} \cdot \mathbf{u}_{1\lambda} = -2\alpha \frac{b_{0x}(v_{Ax} + p_x \mathbf{p} \cdot \mathbf{v}_A / p^2) - \frac{1}{2} \mathbf{b}_0 \cdot \mathbf{v}_A}{|\mathbf{v}_{AT} + \mathbf{b}_0|^2}. \quad (61)$$

$$[\mathbf{b}_1 \cdot (\mathbf{v}_A + \mathbf{b}_0)]_\lambda = \frac{2\alpha}{p^2} \left[p_x b_{0x} + \mathbf{p} \cdot \mathbf{v}_A \left(1 - \frac{\beta}{\cos^2 \theta} \right) \frac{b_{0x}(v_{Ax} + p_x \mathbf{p} \cdot \mathbf{v}_A / p^2) - \frac{1}{2} \mathbf{b}_0 \cdot \mathbf{v}_A}{|\mathbf{v}_{AT} + \mathbf{b}_0|^2} \right]. \quad (65)$$

The physical scenario described by these equations is quite simple: expansion of a nearly-constant- B^2 Alfvén wave (\mathbf{b}_0) constantly drives a small fluctuation in the magnetic pressure $\delta(b^2)_1$ (65); this drives a compressive flow $u_{1\text{comp}}$ (61) which nonlinearly distorts the main Alfvénic fluctuation via (59), keeping the fluctuations in the magnetic pressure small and thus largely preserving the Alfvénic character of the wave.

3. SCALINGS

There are several interesting and simple scaling properties shared by all solutions that can be deduced from Eq. (59) and the expressions for the compressive components (60–65). We examine these in this section.

3.1. Amplitude scaling

First, notice that

$$\begin{aligned} [\mathbf{p} \cdot \mathbf{u}_1(\mathbf{v}_{AT} + \mathbf{b}_0)]_\lambda \cdot \mathbf{b}_0 &= [\mathbf{p} \cdot \mathbf{u}_1(\mathbf{v}_{AT} + \mathbf{b}_0) \cdot \mathbf{b}_0]_\lambda \\ &\quad - \mathbf{p} \cdot \mathbf{u}_1(\mathbf{v}_{AT} + \mathbf{b}_0) \cdot \mathbf{b}_{0\lambda}, \end{aligned} \quad (66)$$

This nonlinear distortion steepens the waveform of \mathbf{b}_0 , maintaining its constant magnetic field strength $|\mathbf{v}_A + \mathbf{b}_0|$, despite its changing amplitude. Related to this compressive velocity, there are density fluctuations

$$\delta\rho_1 = \epsilon\rho_1, \quad (62)$$

given using the continuity equation by Eq. (42), which reads

$$\frac{\rho_1}{\bar{\rho}} = -\frac{\mathbf{p} \cdot \mathbf{u}_1}{\mathbf{p} \cdot \mathbf{v}_A}, \quad (63)$$

as well as magnetic-pressure fluctuations

$$\delta(b^2)_1 = 2\epsilon\mathbf{b}_1 \cdot (\mathbf{v}_A + \mathbf{b}_0), \quad (64)$$

determined in terms of their gradient by Eq. (58), which reads

where the cancellation comes from our assumption (25) that the zeroth order magnetic-field strength is constant. Taking the dot product of Eq. (59) with \mathbf{b}_0 and using (66), we obtain

$$\frac{\partial b_0^2}{\partial \tau} + \alpha \left(b_0^2 + \frac{2\mathbf{p} \cdot \mathbf{b}_0 p_x b_{0x}}{p^2} \right) + [\mathbf{p} \cdot \mathbf{u}_1(\mathbf{v}_{AT} + \mathbf{b}_0) \cdot \mathbf{b}_0]_\lambda = 0, \quad (67)$$

where the cancellation is because $\mathbf{p} \cdot \mathbf{b}_0 = 0$, the expression of $\nabla \cdot \mathbf{B} = 0$ in this one-dimensional system. Upon performing a spatial average of (67) using (20), the nonlinear term vanishes since it is a total derivative, leaving

$$\frac{\partial \overline{b_0^2}}{\partial \tau} = -\alpha \overline{b_0^2}, \quad (68)$$

whose solution is

$$\overline{b_0^2} \propto a^{-1}. \quad (69)$$

This dependence is identical to the WKB solution at low amplitude (Grappin et al. 1993). The only difference is that now it is the *average* amplitude that has the scaling law: this is because the waveform must distort in order

to keep B^2 nearly constant. Then, using (69) and (47), the normalized RMS amplitude, in the case of radial \mathbf{B} , scales as

$$\sqrt{\frac{b_0^2}{v_A^2}} \propto a^{1/2}, \quad (70)$$

i.e., the normalized RMS amplitude increases with a . This is a special case (with the solar wind velocity U constant) of the result previously obtained by Hollweg 1974 (in a more general case with the solar wind velocity $U \neq \text{const.}$ and super-radial expansion of the magnetic field lines) and Barnes & Hollweg 1974 (in a much more general case, without any symmetry). However, these authors did not study explicitly how the wave is distorted by the expansion.

What does this mean (or more generally, what does the Hollweg 1974 result mean) for radial magnetic-field reversals (an important aspect of the observed switchbacks)? To reverse the field, the fluctuation must grow to high amplitude. Let us assume that the source of the Alfvén waves at the coronal base is statistically quite uniform, with a low initial amplitude. Then there are two rather obvious consequences.

First, sufficiently close to the Sun, we should expect the fraction of the volume filled with switchback fluctuations to be an increasing function of R :⁵ the first switchbacks to form are the fluctuations with initially largest amplitude, and as the expansion continues more and more fluctuations can form switchbacks. This is indeed what is seen in the observations (Mozer et al. 2020; Badman et al. 2020), which seems to be strong evidence in support of the *in situ* generation hypothesis (Squire et al. 2020): it is hard to imagine a similar dependence emerging from the mechanisms in which the switchbacks have a lower-coronal origin (Drake et al. 2020; Zank et al. 2020).

Second, going beyond our Eq. (70) and applying the Hollweg (1974) results, we should expect more reversals in regions where larger super-radial expansion of the magnetic field occurs. This reduces \overline{B} , which thus acts to increase $\delta B/\overline{B}$. Thus, switchbacks should be observed in “patches” that are correlated with regions where the expansion has been most significant (e.g. slow

wind), and they should be relatively absent in regions where the expansion has not been as dramatic (e.g. fast wind). This is a specific, falsifiable prediction of the Squire et al. (2020) Alfvén wave expansion model for switchback generation.

3.2. Parallel magnetic field fluctuations

First, we define an additional coordinate system. Let us define unit vectors $\mathbf{n} = \mathbf{p} \times \mathbf{v}_A / pv_A$ and $\mathbf{m} = (\mathbf{p} \times \mathbf{v}_A) \times \mathbf{p} / p^2 v_A$; the mean field \mathbf{v}_A is in the \mathbf{m} - \mathbf{p} plane, and $v_{Am} = v_A \sin \theta$ and $v_{Ap} = v_A \cos \theta$, where θ is the angle between \mathbf{p} and \mathbf{v}_A . Then, the constancy of the zeroth-order transverse (to \mathbf{p}) magnetic field strength, $b_T^2 = |\mathbf{v}_{AT} + \mathbf{b}_0|^2 = \text{const.}$, means that magnetic field fluctuations in the m -direction are related to b_T and the fluctuations in the n -direction by

$$\begin{aligned} b_T^2 &= b_{0n}^2 + (v_{Am} + b_{0m})^2, \\ &= b_{0n}^2 + 2v_{Am}b_{0m} + v_{Am}^2 + b_{0m}^2. \end{aligned} \quad (71)$$

Let us also define the normalized amplitude,⁶

$$A = \frac{1}{v_A} \sqrt{b_{0n}^2 + b_{0m}^2}, \quad (72)$$

and also

$$D = \frac{A}{\sin \theta}. \quad (73)$$

From Eq. 72, we trivially have

$$\frac{b_{0m}}{v_A} \lesssim A. \quad (74)$$

However, for $D \ll 1$, a more restrictive bound applies, which may be derived as follows. In terms of D , Eq. (71) may be written

$$\frac{b_T^2}{v_{Am}^2} = D^2 + 1 + \frac{2b_{0m}}{v_{Am}}. \quad (75)$$

Taking the spatial average of this equation (cf. Eq. 20),

$$\frac{b_T^2}{v_{Am}^2} = \overline{D^2} + 1, \quad (76)$$

and so

$$\frac{b_{0m}}{v_{Am}} = \frac{1}{2} (\overline{D^2} - D^2). \quad (77)$$

Now, let us look at small-amplitude case specifically, $D \ll 1$. If we assume that in terms of scalings, $D^2 \sim \overline{D^2}$, we see that b_{0m}/v_{Am} is second-order in D or smaller (and upon inspecting Eq. (72), b_{0n}/v_{Am} is first-order in

⁵ Probably within a few tens of R_\odot . This is for two reasons; first, further from the Sun the non-radial components of the mean field become more important (the “Parker Spiral”). These decay more weakly with a (cf. Eq. 47), and so the normalised amplitude tends to saturate. Second, further from the Sun, our neglect of nonlinear interaction due to counterpropagating Alfvén waves produced by reflection (i.e. turbulence), as well as parametric decay and/or other instabilities, becomes less justifiable: these would also cause a more significant decay in the fluctuation amplitude.

⁶ Note that this is normalized to the mean field v_A , rather than the total field strength b : A is unbounded, whereas $b_0/b \leq 2$ for a system with b constant (Matteini et al. 2018).

D). Using (72), (73), (77), and $v_{Am} = v_A \sin \theta$, in terms of scaling with A we have

$$\frac{b_{0m}}{v_A} \lesssim \frac{A^2}{\sin \theta}, \quad \text{when } D \ll 1. \quad (78)$$

This relationship is well-known (Barnes & Hollweg 1974; Vasquez & Hollweg 1998). As $D \rightarrow 0$, the polarization of the linearized Alfvén wave is recovered. As $D \rightarrow 1$ from below, (78) matches the less restrictive earlier bound (74); for $D \gtrsim 1$, b_{0m}/v_A is no longer required to be much smaller than b_{0n} , and must merely satisfy (74). Both our scalings (78) and (74) put upper bounds on the scaling of b_{0m} ; the exact relationship between b_{0m} and b_{0n} depends on the waveform. We proceed by assuming that b_{0m} agrees with the scaling corresponding to smallest applicable upper bound⁷.

The component of the fluctuation parallel to the magnetic field $\bar{\mathbf{B}}$ is

$$b_{0\parallel} = b_{0m} \sin \theta, \quad (79)$$

because the angle between \mathbf{p} and \mathbf{v}_A is θ , and \mathbf{m} is perpendicular to \mathbf{p} (the wave is transverse) but in the plane of \mathbf{p} and \mathbf{v}_A . Using the scalings of b_{0m} described above (Eqs. 78 and 74),

$$\frac{b_{0\parallel}}{v_A} \sim \begin{cases} A^2, & D \ll 1 \\ A \sin \theta, & D \gtrsim 1, \end{cases} \quad (80)$$

which matches at $D \sim 1$. In this paper, we will only consider radial \mathbf{v}_A , and so this component of the fluctuations is responsible for magnetic-field reversals. In the following section, we will make use of these scalings to examine the scaling behaviour of the compressive components. Moreover, (80) shows that there is an angular dependence to the propensity of fluctuations to reverse the background field: for a switchback, $b_{0\parallel}/v_A \gtrsim 1$, which is attained at lower amplitude A for perpendicular ($\sin \theta \approx 1$) waves. This may help to explain the observations of Laker et al. (2020), who found that switchbacks have aspect ratios of around 10–30, extremely elongated in the direction of the mean magnetic field.

3.3. Compressive velocity and density fluctuations

Assuming a radial $\mathbf{v}_A = \hat{\mathbf{x}}v_{Ax}$, we may write (61) as

$$p u_{1\text{comp}\lambda} = -2\epsilon\alpha \frac{b_{0x} v_{Ax} (\cos^2 \theta + 1/2)}{b_T^2}. \quad (81)$$

⁷ This will be true in the numerical simulations in Sec. 4, and is true for all simulations we have tried starting with small-amplitude, continuous initial conditions.

Recall that $\alpha/\mathbf{p} \cdot \mathbf{v}_A = 1$ (Eq. 48); then,

$$u_{1\text{comp}\lambda} = -\epsilon (2 \cos^2 \theta + 1) \cos \theta \left(\frac{v_{Ax}^2}{b_T^2} \right) b_{0x}. \quad (82)$$

We can estimate the amplitude of the compressive velocity compared to that of the Alfvénic velocity fluctuations $\mathbf{u}_0 = \mathbf{b}_0$. First, note that if the characteristic width of the waveform in λ is roughly constant, $u_{1\text{comp}\lambda} \sim u_{1\text{comp}}$. Then at low amplitude, $u_0 \ll v_{Ax} \sin \theta$, using (80),

$$\frac{u_{1\text{comp}}}{u_0} \sim \epsilon (2 \cos^2 \theta + 1) \frac{\cos \theta}{\sin^2 \theta} \frac{u_0}{v_{Ax}}, \quad (83)$$

At high amplitude, $u_0 \gg v_{Ax} \sin \theta$, we instead obtain

$$\frac{u_{1\text{comp}}}{u_0} \sim \epsilon (2 \cos^2 \theta + 1) \sin \theta \cos \theta \frac{v_{Ax}^2}{u_0^2}. \quad (84)$$

First, note that the expressions match at $u_0 \sim v_{Ax} \sin \theta$ (i.e. $D \sim 1$), as expected. Second, we see that the compressive velocity scales with ϵ , or equivalently \dot{a} : thus, we might expect more compressive fluctuations in regions which undergo larger expansion. Interestingly, the slow solar wind, which has expanded more, is observed to have a larger compressible fraction (Bruno & Carbone 2013) than the fast wind, which is thought to have expanded less (Wang & Sheeley 1990; Chandran 2021).

Let us assume that the initial propagation angle θ^* at the coronal base where the wave originates is nearly perpendicular, $0 < \cos \theta^* \ll 1$. Then, initially $\cos \theta \sim 1/\tan \theta \sim a/\tan \theta^* \ll 1$ (using Eq. 12). Eventually, θ decreases until $\cos \theta \approx 1$, and instead $\sin \theta \propto 1/a$. Thus, also using $u_0/v_{Ax} \propto a^{1/2}$ (cf. Eq. 68), we expect

$$\frac{u_{1\text{comp}}}{u_0} \propto \begin{cases} a^{3/2}, & D \ll 1 \\ a^{-2}, & D \gg 1. \end{cases} \quad (85)$$

The maximum is therefore reached at approximately $D \sim 1$; thus, $A \sim \sin \theta$ is the characteristic amplitude at which the Alfvén waves are maximally steepened and distorted by the expansion in order to keep B^2 constant.

Via the continuity equation, the density fluctuations have a rather simple relationship with the compressible component of the velocity, given by Eq. (63),

$$\frac{\delta \rho_1}{\bar{\rho}} = -\frac{u_{1\text{comp}}}{v_{Ax} \cos \theta}. \quad (86)$$

Thus, for rather perpendicular waves for which $\cos \theta \ll 1$ (as appears to be the case for switchbacks in the real world, cf. Laker et al. 2020), the density fluctuations should be large compared to the compressive velocity. Given an observational estimate for θ (for example, using a minimum variance analysis), this is a testable prediction of our model.

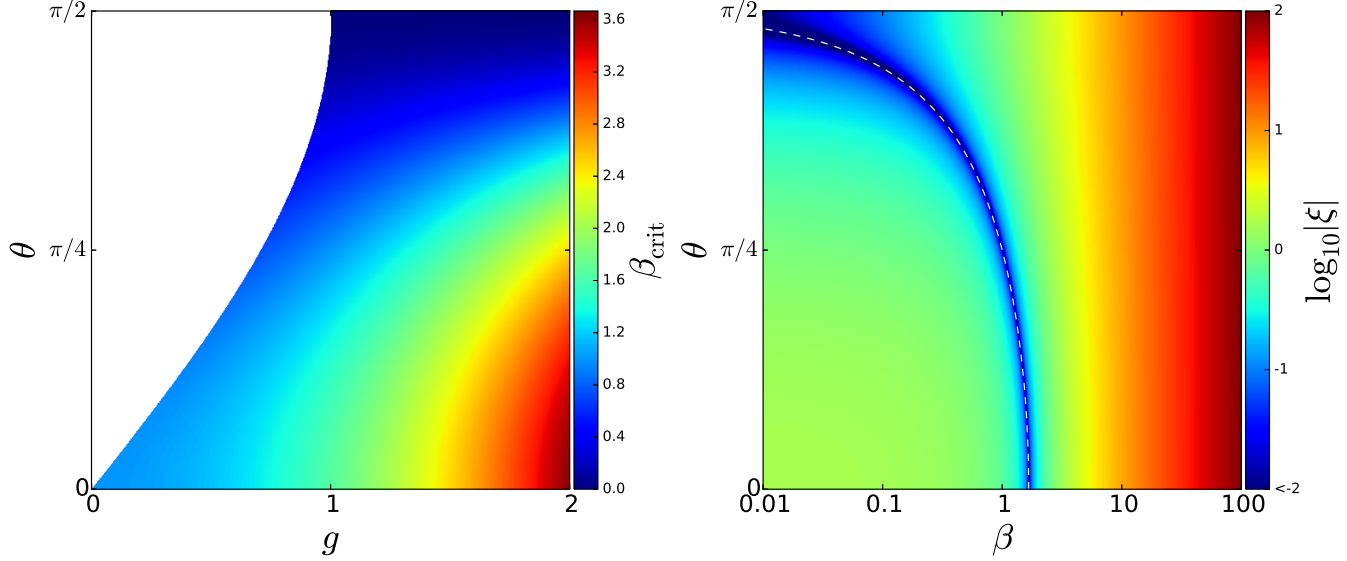


Figure 1. Left: β_{crit} plotted as a function of $g = b_T/v_{Ax}$ and θ . Note that $g \geq \sin \theta$ by geometry; accordingly, the forbidden region is left unfilled on the plot. **Right:** The logarithm of $|\xi|$ (Eq. 90) plotted as a function of β and θ , for $g = 1$; to the left of the white dotted line (which is centered around $\beta = \beta_{\text{crit}}$), $\xi > 0$, while to the right, $\xi < 0$.

3.4. Magnetic field strength fluctuations

The fluctuations in magnetic field strength are given by (65). With radial v_A , this reduces to

$$\frac{1}{2}\delta(b^2)_{1\lambda} = 2\epsilon\alpha \frac{p_x b_{0x}}{p^2} \frac{2b_T^2 + \left(1 - \frac{\beta}{\cos^2 \theta}\right) v_{Ax}^2 (2\cos^2 \theta + 1)}{2b_T^2}. \quad (87)$$

Using (48), we find

$$\frac{\delta(b^2)_{1\lambda}}{v_{Ax}^2} = \epsilon \frac{b_{0x}}{v_{Ax}} \frac{2b_T^2 \cos^2 \theta + (\cos^2 \theta - \beta) v_{Ax}^2 (2\cos^2 \theta + 1)}{b_T^2}. \quad (88)$$

The transverse magnetic field b_T is spatially constant; let us set it equal to $g v_{Ax}$, where g is a function of a that depends on the specific solution. Then, the magnetic pressure fluctuation vanishes if

$$\beta = \beta_{\text{crit}} = \cos^2 \theta + \frac{2g^2 \cos^2 \theta}{2\cos^2 \theta + 1}. \quad (89)$$

As $\theta \rightarrow 0$, $\beta_{\text{crit}} \rightarrow 1 + 2g^2/3$, while as $\theta \rightarrow \pi/2$, $\beta_{\text{crit}} \rightarrow 0$. For $b_0 \sim v_{Ax}$, g is of order unity; thus, the magnetic pressure fluctuations in large-amplitude waves of moderate to parallel θ are always minimized for β of order unity. For clarity, β_{crit} is plotted as a function of g and θ in the left-hand panel of Figure 1; we indeed see that $\beta_{\text{crit}} \sim 1$ apart from close to $\theta = \pi/2$. This explains the numerical observation of Squire et al. (2020), who saw that the magnetic compression $C_{B^2} = \langle \delta(B^2) \rangle / \langle |\delta \mathbf{B}|^2 \rangle$ was indeed minimized in their expanding box turbulence simulations when $\beta \sim 1$. Observationally, there are hints

of a similar effect in Larosa et al. (2020), as we discuss in the next section.

3.5. Compressive component polarization

Larosa et al. (2020) have performed a statistical analysis of 70 switchbacks, and found that in some the density and field-strength fluctuations have the same sign, but in others they have opposite sign. This may be a natural consequence of the β -dependence identified in the previous section. Use Eqs. (82), (86) and (88) to form the polarization ratio

$$\begin{aligned} \xi &= \frac{\delta(b^2)_{1\lambda}/v_{Ax}^2}{\rho_{1\lambda}/\bar{\rho}} \\ &= \frac{2(b_T^2/v_{Ax}^2) \cos^2 \theta + (\cos^2 \theta - \beta) (2\cos^2 \theta + 1)}{2\cos^2 \theta + 1}. \end{aligned} \quad (90)$$

For $\beta < \beta_{\text{crit}}$, $\xi > 0$, while for $\beta > \beta_{\text{crit}}$, $\xi < 0$. This is plotted in the right-hand panel of Figure 1: we plot $\log_{10} |\xi|$ as a function of β and θ , choosing $g = 1$ (appropriate for moderately large-amplitude waves). The blue band around β_{crit} (shown as a dashed white line) is the region where the magnetic-field-strength fluctuations are very low; to the left of this band (low β), $\xi > 0$ and tends to a constant as $\beta \rightarrow 0$; while to the right (high β), $\xi < 0$ and is unbounded ($\xi \propto \beta$) as $\beta \rightarrow \infty$. Thus, it is potentially the combination of β and propagation angle that causes the highly variable behaviour in the observations. It should be possible to diagnose θ in the data using a minimum variance analysis, which

would make a test of this hypothesis possible. Given that we have restricted ourselves to a locally isothermal equation of state, it is unlikely that (90) will be reproduced exactly. For example, Farrell et al. (2020) found opposite trends in pressure and density across switchback boundaries, which is impossible with our isothermal model. However, the basic principle involved, that β and θ will affect the polarization of the compressive components of the wave, should remain valid.

This transition also appears in the early work of Cohen & Kulsrud (1974), who studied the relaxation of quasi-parallel, low-amplitude waves to constant- B^2 Alfvénic states. In their theory, it appears as a singularity: at $\beta = 1$, their evolution becomes infinitely fast (violating their assumptions) because their fluctuations in magnetic field strength are imposed as an initial condition only. In our case, the effect is much less harmful because $\delta(b^2)_1$ is generated only by the expansion: physically, the interpretation is that around $\beta = \beta_{\text{crit}}$, the wave is able to remove $\delta(b^2)_1$ very efficiently.

4. EXAMPLE SOLUTIONS

To illustrate the properties of the wave more concretely, we solve (59) numerically. We use a pseudospectral method with $n_\lambda = 16384$ grid points, and $\Lambda = 2\pi$, with an initial condition \mathbf{b}_0^* at $\tau = 0$, and the compressive components calculated according to Eqs. (60–65). We take \mathbf{p} in the x - y plane. We impose white noise in b_{0n}^* in the $\mathbf{n} = \mathbf{p} \times \mathbf{v}_A / pv_A$ direction, low-pass filtered to keep only the first 200 harmonics. To this, we add another component of the magnetic field in the $\mathbf{m} = (\mathbf{p} \times \mathbf{v}_A) \times \mathbf{p} / p^2 v_A$ direction to make this initial condition into a constant- B^2 Alfvén wave:

$$b_{0m}^* = -v_{Ax}^* \sin \theta^* + \sqrt{C^2 - b_{0n}^{*2}}, \quad (91)$$

so that the initial transverse magnetic field strength is a constant in λ , C . We must choose C so that $\langle b_{0m}^* \rangle = 0$; this can be achieved by iteration, provided that the initial D^* (cf. Eq. 73) is sufficiently small (Barnes & Hollweg 1974). This initial condition mimics the random, volume-filling Alfvén waves that are present in the solar wind (bearing in mind we are limited to one dimensional MHD waves, and additionally neglect turbulence and instability).

There are various parameter choices which apply to all simulations presented here. We take the mean magnetic field to be radial, $\overline{\mathbf{B}} = \hat{\mathbf{x}} \overline{B}_x$. The normalized amplitude (cf. Eq. 72) of the initial waveform is chosen to be small, with root-mean-square (RMS) value $A_{\text{rms}}^* = 0.03$. We choose $\epsilon = 0.1$, corresponding roughly to the observed switchbacks at the orbit of PSP (Laker et al. 2020).

We must also choose the initial angle between \mathbf{p} and \mathbf{v}_A , θ^* . As the evolution progresses, θ evolves as (cf. 12, and remembering that we impose radial \mathbf{v}_A)

$$\tan \theta = \frac{\tan \theta^*}{a}, \quad (92)$$

so that the wave evolves into more parallel propagation with time. To achieve a particular θ_{target} when the wave attains a particular rms amplitude A_{target} , we use Eqs. (68) and (92), and choose

$$\theta^* = \arctan \left[\left(\frac{A_{\text{target}}}{A_{\text{rms}}^*} \right)^2 \tan \theta_{\text{target}} \right]. \quad (93)$$

4.1. Comparison with observations

First, we perform a simulation intended to roughly match the Laker et al. (2020) observations, which found that the observed aspect ratio of switchback structures at the orbit of PSP was around 30. Thus, we choose

$$\tan \theta_{\text{target}} = 30, \quad A_{\text{target}} = 1, \quad (94)$$

so that the wave is large-amplitude at θ_{target} .⁸ Using Eq. (93), this means that $\tan \theta^*$ is extremely large. This probably implies that there must be additional physics involved in the observed large aspect ratio of switchbacks observed by Laker et al. (2020), beyond the simple one-dimensional model presented here (note also that the initial condition is not supposed to correspond accurately to conditions at the coronal base; the EBM is an extremely poor approximation there). However, the solution to our equations that attains $A \sim 1$ at $\tan \theta_{\text{target}} = 30$ may provide some guidance as to the properties of the observed spherically-polarized switchbacks at the orbit of PSP. This solution is plotted at different A_{rms} in Figure 2. In its initial state, the wave has only a very small radial field fluctuation (cf. Eq. 78); however, once it attains a larger normalized amplitude, the radial fluctuations become relatively large, at some locations reversing the direction of the radial field and creating switchbacks. Superficially, the waveform looks somewhat similar to PSP data (see, for example, Fig. 1 of de Wit et al. 2020).

To make this comparison more quantitative, we show in Figure 3 the fraction of reversed radial magnetic field (a.k.a. “switchback fraction”, F_{sb}) as a function of the normalized amplitude for this simulation. For $A \approx 1$, $F_{\text{sb}} \approx 0.04$, while for $A \approx 1.5$, $F_{\text{sb}} \approx 0.13$: those amplitudes are compatible with the amplitude of the fluctuations at PSP. Thus, the observed 6% of the volume

⁸ $A = 1$ is probably a lower bound on the observed fluctuation amplitude at the first few PSP perihelia.

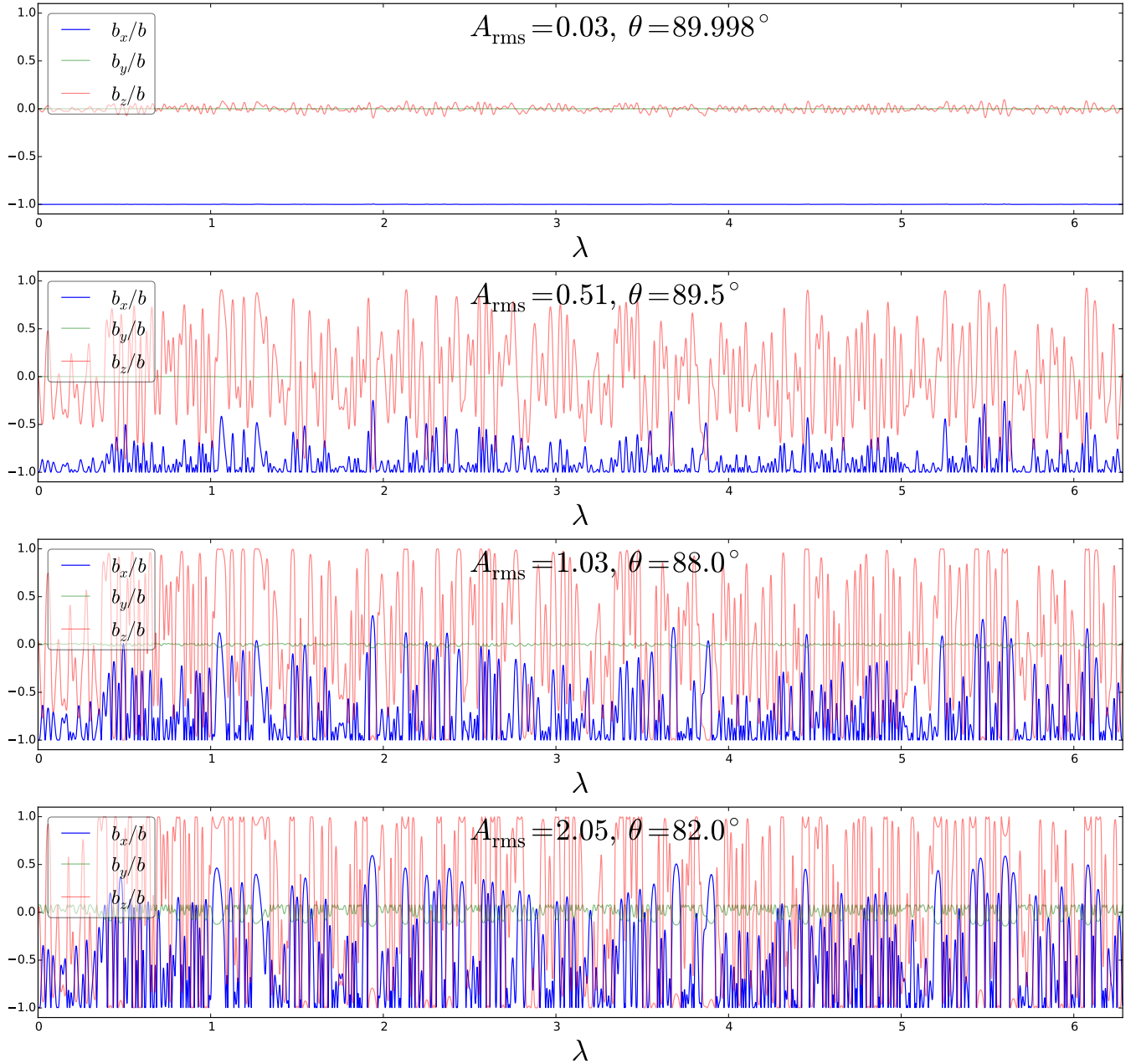


Figure 2. Evolution of white noise with initial angle determined by (93) using parameters (94) chosen to approximately match observations, shown at four different times at which the RMS amplitude is $A_{\text{rms}} = 0.03, 0.51, 1.03, 2.05$, top to bottom. The angle θ between \mathbf{p} and \mathbf{v}_A is also shown for each time. The x , y , and z components of the primary Alfvén wave \mathbf{b}_0 are shown in blue, green and red respectively, normalized by the total (zeroth-order) magnetic field strength b .

filled by switchbacks at the orbit of PSP (Badman et al. 2020) appears to be compatible with simply a collection of randomly phased, large-amplitude AW and does not need any particular special event in the corona. Moreover, the amplitude increases with radial distance from the Sun (cf. Eqs. 68 and Hollweg 1974), which then means that the switchback fraction does also: this is also observed (Badman et al. 2020; Mozer et al. 2020), and would be hard to explain if the structures already

reversed the radial field at the point they were generated in the corona (Drake et al. 2020; Zank et al. 2020). However, there is another parameter that is not taken into account in Fig. 3, the angle θ . We examine the effect this has on the propensity to form switchbacks next.

4.2. Effect of θ

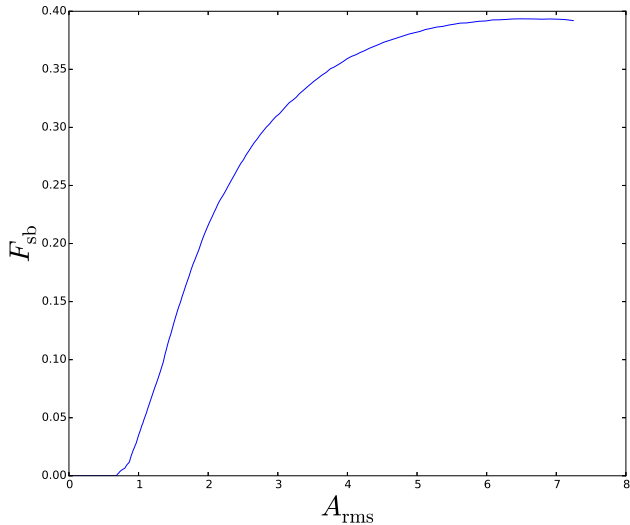


Figure 3. Evolution of the switchback fraction F_{sb} with amplitude, for the solution shown in Fig. 2.

For the simulation shown in Fig. 2, θ remains close to 90° until very late times (large amplitudes). It is very interesting to look at what happens for structures that have a less extreme θ^* , and thus attain a smaller θ when $A_{\text{rms}} = 1$. For example, in Fig. 4 we show results from a simulation with

$$\tan \theta_{\text{target}} = 1, \quad A_{\text{target}} = 1, \quad (95)$$

but the same b_{0n}^* as before: i.e., much less oblique at $A_{\text{rms}} = 1$. Now, there are no switchbacks at any point in the evolution. This is simply because of the relationship derived in Sec. 3.2: according to Eq. (80), the normalized amplitude of the parallel (radial in this case) fluctuations is smaller than A by a factor $\sin \theta$. Also visible at late times is the large b_{0y} component: again, this is because \mathbf{p} rotates towards the x -direction, and $\mathbf{p} \cdot \mathbf{b}_0 = 0$ (Eq. 30). Figure 5 shows the RMS parallel (radial, since \mathbf{B} is in the x -direction) component of the fluctuation, $b_{0x,\text{rms}}$ as a function of A_{rms} . At small amplitudes, $b_{0x,\text{rms}} \sim A_{\text{rms}}^2$, while once the amplitude becomes large and θ decreases, $b_{0x,\text{rms}} \sim A_{\text{rms}} \sin \theta$. This agrees with Eq. (80) in both limits, providing some validation for the scaling analysis in Sec. 3.2.

To test this scaling analysis more thoroughly, we perform a suite of simulations, with $A_{\text{target}} = 1$, and vary θ_{target} from $\pi/8$ to $\pi/2$ in steps of $\pi/400$. We then calculate $F_{\text{sb}}(a)$, $A_{\text{rms}}(a)$, and $\theta(a)$ for each of these solutions, and interpolate between them in the $A_{\text{rms}}-\theta$ plane to estimate $F_{\text{sb}}(A_{\text{rms}}, \theta)$. This is shown in Fig. 6, and shows that switchbacks do form more readily for more perpendicular fluctuations: moreover, the contours of F_{sb} roughly agree with the prediction of Eq. (80) that

the propensity to form radial magnetic-field reversals depends on $A \sin \theta$.⁹

4.3. Steepening

In Sec. 3.3, we estimated the relative amplitude of the small compressive velocity fluctuations $u_{1\text{comp}}$ and the primary Alfvénic velocity fluctuation u_0 (Eqs. 83 and 84). This estimate predicts opposite scalings in the small- and high-amplitude limits, and a maximum where $D = A/\sin \theta \sim 1$ (see Eq. 73). We can test this with our simulations. Specifically, we use the simulation with the less perpendicular initialization (95), whose zeroth-order waveform is shown in Fig. 4. The normalized compressive velocity is plotted in Fig. 7, and it agrees well with our scaling in both limits. Moreover, the maximum is attained, as expected, when $D_{\text{rms}} \sim 1$. This shows that the majority of the steepening occurs when $A_{\text{rms}} \sim 1/\sin \theta$, i.e. at moderate normalized amplitude, and at a particular propagation angle.

A more direct way of looking at the steepening is to examine how the gradients of the primary waveform evolve with time. To do so, we define the “steepening factor”

$$Q = \frac{|\mathbf{b}_{0\lambda}|^2/|\mathbf{b}_0|^2}{|\mathbf{b}_{0\lambda}^*|^2/|\mathbf{b}_0^*|^2}, \quad (96)$$

which measures how steep, on average, gradients are compared to the initial condition. We perform a second suite of simulations, now taking

$$\theta^* = \arctan \left(\frac{\sin^2 \theta_{\text{target}} \tan \theta_{\text{target}}}{A^2} \right), \quad (97)$$

where θ_{target} now runs from $\pi/20$ to $\pi/2$ in steps of $\pi/100$. This initialization means that $D_{\text{rms}} = 1$ (see Eq. 73) when $\theta = \theta_{\text{target}}$. We calculate $Q(a)$, $A_{\text{rms}}(a)$, $\theta(a)$ for each simulation, and interpolate between them in the $A_{\text{rms}}-\theta$ plane to estimate $Q(A_{\text{rms}}, \theta)$. This is plotted in Figure 8. The contours of Q , as expected, are lines of constant D . This could be tested if a variety of propagation angles could be diagnosed in the data: the large switchbacks appear to be mainly perpendicular, but deflections of the radial field with smaller amplitude could potentially have smaller θ (and may, according to this analysis, be more steepened).

However, Q remains quite small for all the simulations. This is in stark contrast to the observed switchbacks (e.g. those in the statistical survey of Larosa et al. 2020); many of these exhibit extremely steep rotations at

⁹ A detailed analysis shows that the slight difference is caused by the distortion of the waveform; $\max(A)$ scales slightly differently from A_{rms} .

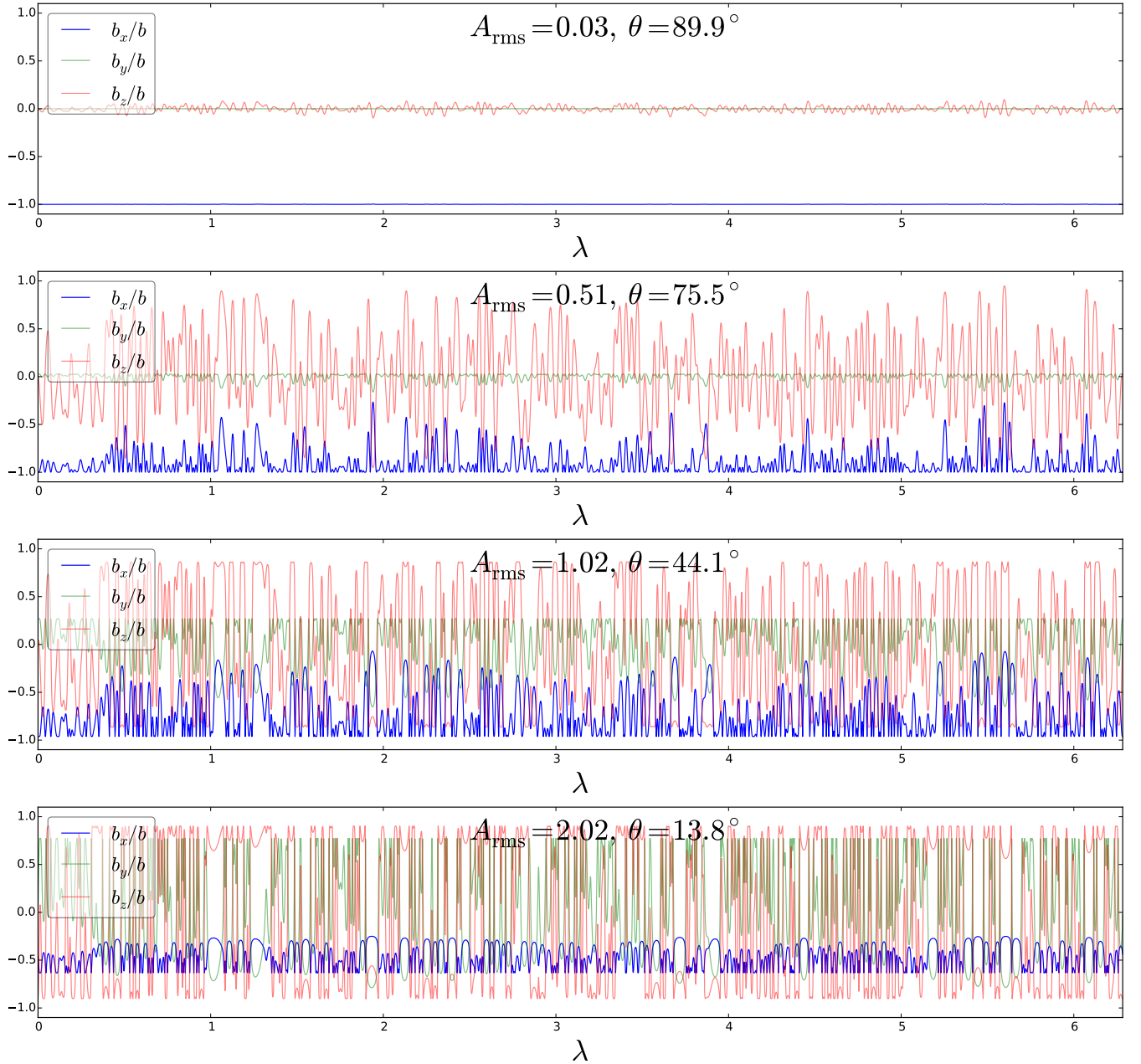


Figure 4. Evolution of white noise with initial angle determined by (93) using parameters (94) chosen to approximately match observations, shown at four different times at which the RMS normalized amplitude is $A_{\text{rms}} = 0.03, 0.51, 1.03, 2.05$, top to bottom. The angle θ between \mathbf{p} and \mathbf{v}_A is also shown for each time. The x , y , and z components of the primary Alfvén wave \mathbf{b}_0 are shown in blue, green and red respectively, normalized by the total (zeroth-order) magnetic field strength b .

their boundaries. Thus, our model cannot explain this property, and additional physics (potentially either due to the effect of three dimensions or kinetics) is required. It should be noted that the switchbacks produced in the MHD turbulence simulations of Squire et al. (2020) and Shoda et al. (2021) do not appear to be significantly steeper than in our model, which may suggest a kinetic origin to the sharp boundaries observed in the

real world; but this could also just be due to the limited resolution available in 3D turbulence simulations.

4.4. Compressive fluctuations: effect of β

From Eqs. (59) and (61), β does not affect the primary Alfvén wave at all, only entering through the relationship between $\delta(b^2)_{1\lambda}$ and the other variables (see Sec. 3.5). For completeness, we plot the compressive fluctuations from the solution in Fig. 4 when it attains

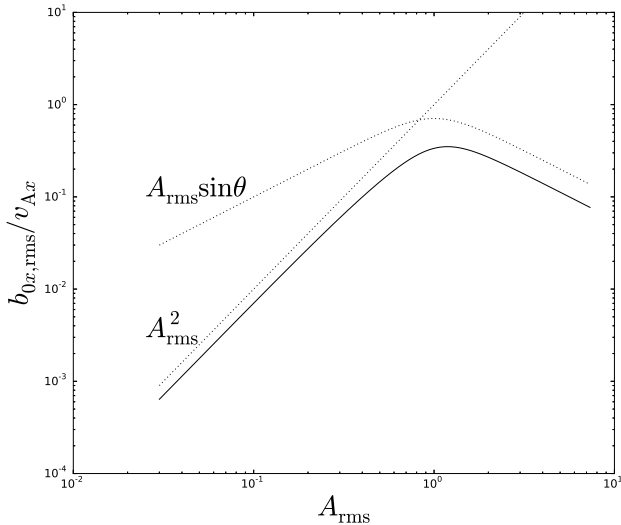


Figure 5. The parallel magnetic-field fluctuation $b_{0x,rms}/v_{Ax}$ (solid line), for the simulation shown in Fig. 4. Dotted lines show the two scaling predictions from Eq. (80).

$A = 1.02$ and $\theta = 44.1^\circ$ at three different $\beta = 0, 1.25, 5$ in Figure 9. Apart from $\delta(b^2)_1$, the solution does not depend on β . At low β , the correlation between $\delta(b^2)_1$ and $\delta\rho_1$ is positive, but at high β , the correlation reverses and $\delta(b^2)_1$ becomes very large relative to the other components, as we deduce in Sec. 3.5. Between these two limits, at $\beta = 1.25 \approx \beta_{crit}$, $\delta(b^2)_1$ is very small compared to u_{1comp} and $\delta\rho_1$: as expected, for moderate θ , the magnetic-field-strength fluctuations become very small for $\beta \sim 1$.

5. EXTENSIONS AND FURTHER WORK

There are several extensions to this work that can and should be performed, relaxing some of the idealized assumptions involved. First, it would be very interesting to go beyond the EBM and investigate the effects of a more realistic expansion model. We plan to investigate the effects of superradial expansion as well as turbulence in a forthcoming work (Mallet et al. 2021).

For the current paper, we have assumed an exactly radial mean magnetic field. Our main dynamical equation (59) and the expressions for the compressible components (61–65) are valid for the mean field in an arbitrary direction, and we plan to investigate the effects of including a Parker spiral (nonzero v_{Ay}) in the future. Two interesting effects emerge: first, the degeneracy between the two directions transverse to radial is removed, which could have implications for the observed distribution of switchbacks; second, the transverse components of the mean magnetic field decay more slowly, which will eventually stop the growth in normalized amplitude, as

well as rotating the wave back into nearly perpendicular propagation.

As we mentioned in the introduction, we have not checked the stability of the wave: it is well-known that the Alfvén wave is unstable to parametric decay (Derby 1978; Del Zanna 2001; Tenerani & Velli 2013). Based on numerical simulations, it appears that this may be somewhat suppressed for localised structures like switchbacks (Tenerani et al. 2020), but this process should again be investigated in the future.

Our analysis is formally one-dimensional, and thus it is only truly valid in regions where the gradient direction is not changing too fast, $\|\nabla\mathbf{p}\|/p^2 \ll 1$. Perfect Alfvénic states of arbitrary amplitude in a homogeneous medium propagate without distortion regardless of their three-dimensional structure, because the group velocity is along \mathbf{v}_A . However, an attempt to generalize our analysis to three-dimensions causes new terms to appear due to a non-zero $\nabla\mathbf{p}$: this couples together different directions, and leads to a three-dimensional turbulent cascade. This may lead to more dramatic discontinuities appearing, due to large local fluctuations in B^2 (cf. Cohen & Kulsrud 1974, although their analysis only formally applies at small-amplitude and parallel propagation). It is, however, encouraging that some of our scaling results seem to apply to the three-dimensional simulations in Squire et al. (2020).

We have assumed a locally isothermal equation of state. This does not seem to be sufficient to explain the data, where pressure and density across switchback boundaries have different dependencies (Farrell et al. 2020). This limitation may be possible to fix within the framework of MHD, because the compressive components of the wave are small. A more interesting problem would be the case where the pressure can be anisotropic: Squire et al. (2016) show that in this case, magnetic-field-strength fluctuations tend to collapse to sharp discontinuities due to nullification of the magnetic tension at the boundary. Interestingly, Woodham et al. (2020) find that the parallel ion temperature seems to be enhanced in switchback patches, showing that it is probably important to incorporate these effects. Additionally, in the data there is often a proton beam moving at an appreciable fraction of \mathbf{v}_A ; this also alters the local Alfvén speed (Barnes & Suffolk 1971), and may in fact be driven by phase-steepened Alfvén waves themselves (González et al. 2021): this could also potentially cause additional nonlinear steepening of the wave.

One additional limitation of our approach is that we have assumed without derivation that to leading order the initial condition is spherically polarized to lowest order. However, so long as the initial condition has a small

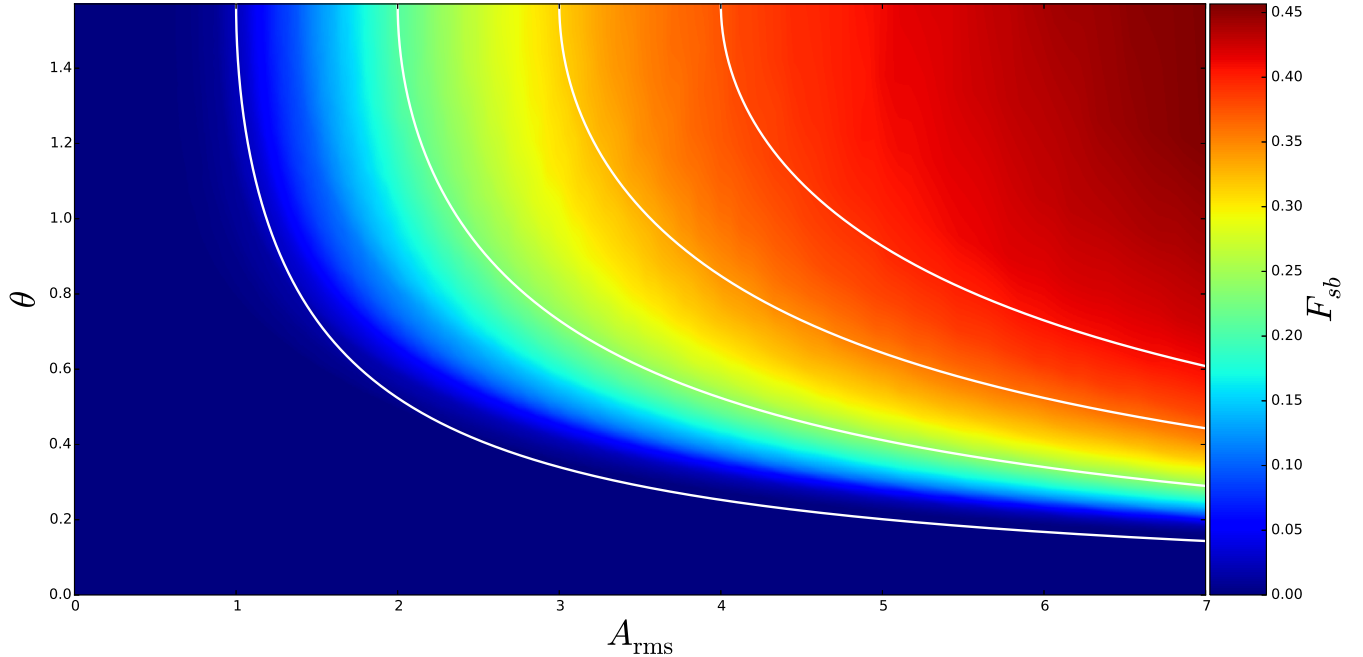


Figure 6. The switchback fraction F_{sb} attained by white-noise solutions as a function of A_{rms} and θ . White lines show, from left to right, $A_{\text{rms}} \sin \theta = 1, 2, 3, 4$ (see Eq. 80).

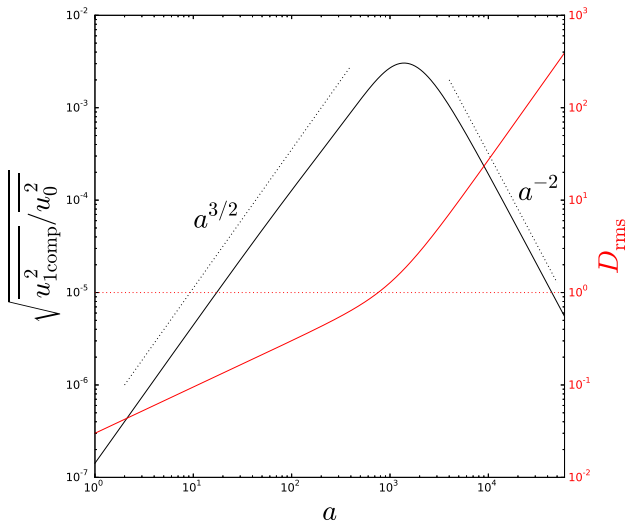


Figure 7. Solid black line: RMS $u_{1\text{comp}}/u_0$ as a function of the expansion factor a , from the solution whose zeroth-order waveform is shown in Fig. 4. Dotted lines show the dependencies in Eq. (85). Solid red line: D_{rms} as a function of a for the same solution. $D_{\text{rms}} = 1$ is marked as a horizontal red dotted line.

amplitude, this is not too restrictive. For propagation close to parallel ($D \gtrsim 1$ while $A \ll 1$), the mechanism of Cohen & Kulsrud (1974) will apply, and the wave will relax smoothly to an exactly constant- B^2 state. For more perpendicular propagation, a small-amplitude fluctua-

tion polarized like a linear Alfvén wave may be written as the sum of a small-amplitude constant- B^2 Alfvén wave and a small-amplitude fast wave (Barnes & Hollweg 1974); the latter, due to the significant propagation angle θ^* , will quickly separate from the former (and dissipate due to either steepening into a shock or, in a collisionless plasma, damping): thus, after a short time, only a small-amplitude constant- B^2 Alfvén wave will remain (this mechanism was first advanced by Barnes & Hollweg 1974 to explain the Alfvénicity of the solar wind). Thus, the evolution of small amplitude waves towards a state of constant B^2 is reasonably well understood, at least in a homogeneous, non-expanding plasma. This evolution could be analyzed within a more comprehensive, future version of the model we have developed, but we expect that such a model would lead to conclusions similar to those we have drawn here.

6. CONCLUSIONS

In this paper, we have developed a basic theory of the evolution of large-amplitude Alfvén waves in the expanding solar wind. Our analysis allows us to make several testable predictions, summarized in Table 1. Some of these predictions appear to match hitherto unexplained facets of both spacecraft observations of switchbacks (e.g. Laker et al. 2020; Larosa et al. 2020; Badman et al. 2020) and numerical simulations of expanding Alfvénic turbulence (Squire et al. 2020); thus, the

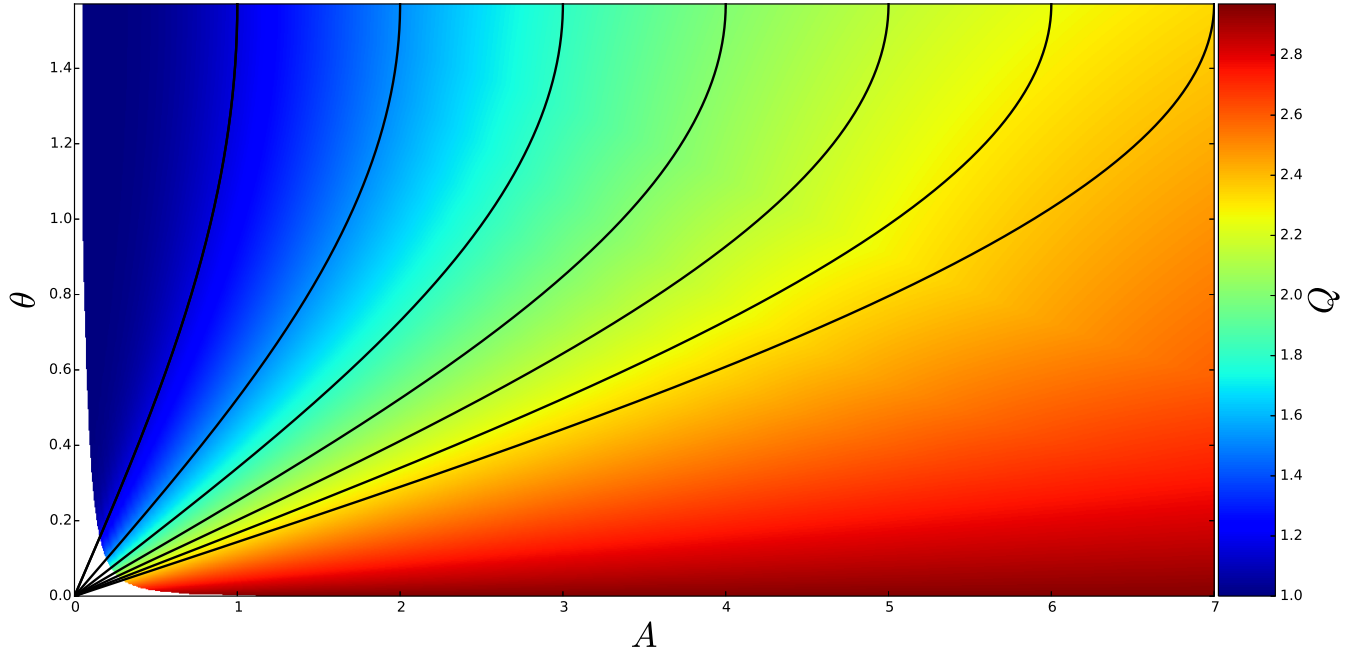


Figure 8. The steepness Q (Eq. 96) as a function of A and θ . Black lines show, from left to right, $D = 1, 2, \dots, 7$.

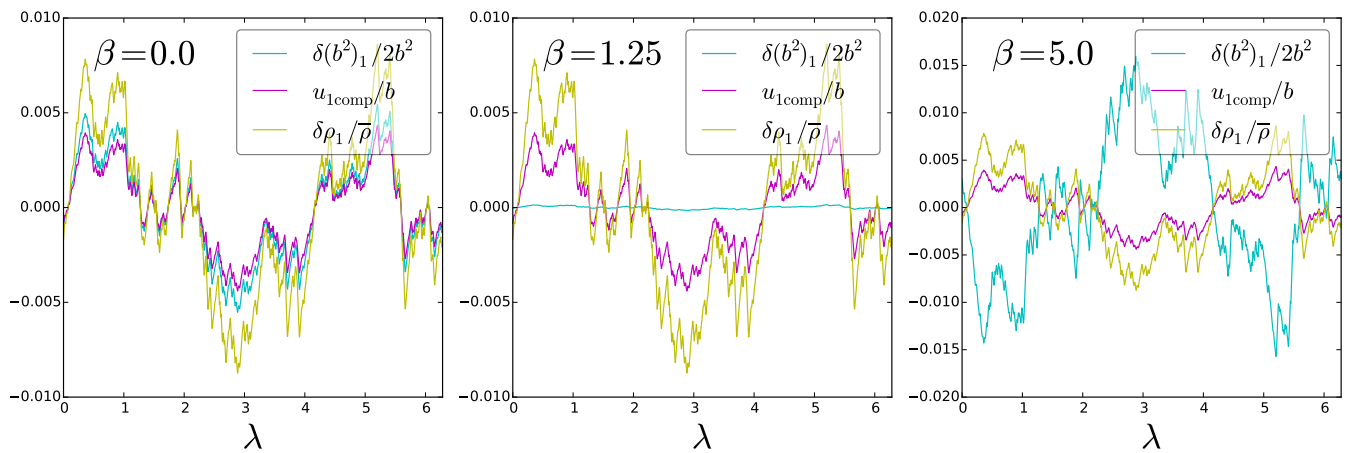


Figure 9. The compressive components for the solution shown in the second panel of Fig. 4, with $A_{\text{rms}} = 1.02$ and $\theta = 44.1^\circ$ with $\beta = 0, 1.25, 5$, left to right. Lines show magnetic-field-strength fluctuations $\delta(b^2)_1$ (cyan), compressive flow $u_{1\text{comp}}$ (pink), density fluctuations $\delta\rho_1/\rho$ (yellow), with the first two normalized by b .

physics encoded in our highly idealized setup seems to be relevant in reality.

At a basic level, the physical behaviour encoded in our “switchback equation” (59) is as follows: expansion increases the normalized amplitude of the wave (Sec. 3.1), pushing it slightly out of its Alfvénic $B^2 = \text{constant}$ state. This slight fluctuation in B^2 drives a compressive flow, opposing the non-constant- B^2 , and distorting the waveform to keep the fluctuation in B^2 small and under control as the plasma expands. We show that this distortion reaches a maximum when the normalized amplitude

$A = \delta B/\bar{B} \approx \sin\theta$, where θ is the angle between the propagation direction and the mean field $\bar{\mathbf{B}}$ (Sec. 3.3). However, comparing this distortion with the observed statistical properties of switchbacks (e.g. the relative width of switchback boundaries and cores observed by Larosa et al. 2020), it does appear that our solutions are not discontinuous enough: thus, there must be additional physics involved; for example, we may need to consider kinetic effects which may enhance steepening due to modifications to the Alfvén velocity from pressure anisotropy and/or beams (Barnes & Suffolk 1971),

or there could be three-dimensional effects that favour the production of more dramatic discontinuities.

We derive analytic expressions for small compressive components of the wave driven by the expansion, in terms of the primary Alfvénic component. All these compressive components scale with the expansion rate: this agrees with the turbulence simulations of [Squire et al. \(2020\)](#), who found that higher expansion rates produced larger fluctuations in the magnetic field strength (“magnetic compressions”). Moreover, we show that the normalized density fluctuations (Eq. 86) are relatively large compared to the normalised compressive velocity when the wave is more perpendicular; this could be tested if the switchbacks can have their direction of propagation diagnosed using a minimum variance analysis. We also show that the small magnetic-field-strength fluctuations vanish at a particular critical β_{crit} , which generically is of order unity (Sec 3.4): this hitherto unexplained phenomenon was also observed by [Squire et al. \(2020\)](#) in the simulations, and thus it seems that our mechanism for achieving this may be at least somewhat applicable in a more complex and realistic scenario. β_{crit} depends on θ , and our prediction for the relationship between θ , β , and the amplitude of fluctuations in the magnetic field strength could be tested using observational data and/or numerical simulations. Connected with this result, we show that the relative phase between the density and magnetic-field-strength fluctuations reverses at β_{crit} (Sec. 3.5): this may be connected to the wide range of polarizations observed in real switchbacks by [Larosa et al. \(2020\)](#), and is another testable quantitative prediction.

We also make predictions regarding the large-amplitude Alfvénic (i.e. constant- B^2) component of the wave. The overall RMS amplitude scales with the total expansion of the plasma: thus, one might expect patches of switchbacks in regions where the plasma has expanded more ([Bale 2021](#)), and the switchback fraction should initially increase with radial distance from the sun, as observed ([Badman et al. 2020](#); [Mozer et al. 2020](#)). We show several solutions of Eq. (59) in Sec. 4, showing that switchbacks can form from sufficiently large-amplitude Alfvén waves, so long as they are sufficiently perpendicular. This preference for perpendicular switchbacks arises simply due to geometry (Sec. 3.2), and is a consequence of the transverse nature of the fluctuations. This

may explain the interesting observation of [Laker et al. \(2020\)](#) that switchbacks appear to be highly elongated (by a factor of 10-30) along the magnetic-field direction. Similar physics seems to occur in the numerical simulations: [Squire et al. \(2020\)](#) observed that the switchbacks were quite perpendicular structures, and also that initial conditions with more modes close to perpendicular were more prone to generating switchbacks. From our analysis, it appears that the initial condition at the coronal base needs to be spectacularly perpendicular to generate substantial switchbacks. The available data ([De Pontieu et al. 2007](#)) does suggest that the initial condition is very perpendicular, but, to match the observed statistics of switchbacks, the evolution of perpendicular and parallel length-scales of the (3D) switchbacks must be significantly different than in our (1D) model. This could potentially arise as a natural consequence of turbulence ([Goldreich & Sridhar 1995](#)).

In summary, it appears that certain features of the switchbacks can be explained in terms of the nonlinear evolution of Alfvén waves as they travel outwards in the expanding solar wind. However, more work is needed to explain the remarkably sharp switchback boundaries in the data, as well as to explain how the switchbacks remain so perpendicular to the mean magnetic field. The main result of our analysis is that although expansion introduces fluctuations in B^2 that might naively be expected to destroy the Alfvénic state, nonlinearly, these are kept under control by distortion of the primary Alfvénic waveform. This provides substantial support for the [Squire et al. \(2020\)](#) model of switchback generation, that they are simply the result of the expansion-driven evolution of initially small-amplitude Alfvénic fluctuations.

- 1 AM would like to thank J. Bonnell, S. Badman,
- 2 M. McManus, and R. Meyrand for helpful comments
- 3 and discussions. AM was supported by NASA grant
- 4 80NSSC21K0462. Support for JS and RM was provided
- 5 by Rutherford Discovery Fellowship RDF-U001804 and
- 6 Marsden Fund grant UOO1727, which are managed
- 7 through the Royal Society Te Apārangi. BDGC was
- 8 supported in part by NASA grants NNX17AI18G and
- 9 80NSSC19K0829. We acknowledge support from NASA
- 10 contract NNN06AA01C.

REFERENCES

Badman, S. T., Bale, S. D., Rouillard, A. P., et al. 2020,
arXiv preprint arXiv:2009.06844
Bale, S.D., e. a. 2021, in preparation

Bale, S., Badman, S., Bonnell, J., et al. 2019, Nature, 576,

- Barnes, A., & Hollweg, J. V. 1974, *J. Geophys. Res.*, 79, 2302
- Barnes, A., & Suffolk, G. C. 1971, *J. Plasma Phys.*, 5, 315
- Belcher, J. W., & Davis, Jr., L. 1971, *J. Geophys. Res.*, 76, 3534, doi: [10.1029/JA076i016p03534](https://doi.org/10.1029/JA076i016p03534)
- Bruno, R., & Carbone, V. 2013, *Living Rev. Solar Phys.*, 10, 2, doi: [10.12942/lrsp-2013-2](https://doi.org/10.12942/lrsp-2013-2)
- Chandran, B. D. 2021, arXiv preprint arXiv:2101.04156
- Chandran, B. D., & Perez, J. C. 2019, *J. Plasma Phys.*, 85
- Cohen, R. H., & Kulsrud, R. M. 1974, *Phys. Fluids*, 17, 2215
- Cranmer, S., & Van Ballegooijen, A. 2005, *Astrophys. J. Suppl. Ser.*, 156, 265
- De Pontieu, B., McIntosh, S., Carlsson, M., et al. 2007, *Science*, 318, 1574
- de Wit, T. D., Krasnoselskikh, V. V., Bale, S. D., et al. 2020, *Astrophys. J. Suppl. Ser.*, 246, 39
- Del Zanna, L. 2001, *Geophys. Res. Lett.*, 28, 2585
- Derby, N. 1978, *Astrophys. J.*, 224, 1013
- Drake, J. F., Agapitov, O., Swisdak, M., et al. 2020, arXiv e-prints, arXiv:2009.05645. <https://arxiv.org/abs/2009.05645>
- Farrell, W. M., MacDowall, R. J., Gruesbeck, J., Bale, S., & Kasper, J. C. 2020, *Astrophys. J. Suppl. Ser.*, 249, 28
- Goldreich, P., & Sridhar, S. 1995, *Astrophys. J.*, 438, 763, doi: [10.1086/175121](https://doi.org/10.1086/175121)
- Goldstein, M. L., Klimas, A., & Barish, F. 1974, *Solar Wind III*, 385
- González, C., Tenerani, A., Matteini, L., Hellinger, P., & Velli, M. 2021, arXiv preprint arXiv:2104.02540
- Grappin, R., & Velli, M. 1996, *J. Geophys. Res. Space Phys.*, 101, 425
- Grappin, R., Velli, M., & Mangeney, A. 1993, *Phys. Rev. Lett.*, 70, 2190
- Hollweg, J. V. 1974, *J. Geophys. Res.*, 79, 1539
- Horbury, T. S., Woolley, T., Laker, R., et al. 2020, *Astrophys. J. Suppl. Ser.*, 246, 45
- Kasper, J., Bale, S., Belcher, J. W., et al. 2019, *Nature*, 576, 228
- Krasnoselskikh, V., Larosa, A., Agapitov, O., et al. 2020, *Astrophys. J.*, 893, 93
- Laker, R., Horbury, T. S., Bale, S. D., et al. 2020, arXiv preprint arXiv:2010.10211
- Larosa, A., Krasnoselskikh, V., de Wit, T. D., et al. 2020, Switchbacks: statistical properties and deviations from alfvénicity. <https://arxiv.org/abs/2012.10420>
- Mallet, A., Squire, J., Chandran, B. D. G., et al. 2021, in preparation
- Matteini, L., Stansby, D., Horbury, T., & Chen, C. H. 2018, *Astrophys. J. Lett.*, 869, L32
- McManus, M. D., Bowen, T. A., Mallet, A., et al. 2020, *Astrophys. J. Suppl. Ser.*, 246, 67
- Mozer, F., Agapitov, O., Bale, S., et al. 2020, *Astrophys. J. Suppl. Ser.*, 246, 68
- Parker, E. 1965, *Space Sci. Rev.*, 4, 666
- Perez, J. C., & Chandran, B. D. G. 2013, *Astrophys. J.*, 776, 124, doi: [10.1088/0004-637X/776/2/124](https://doi.org/10.1088/0004-637X/776/2/124)
- Ruffolo, D., Matthaeus, W. H., Chhiber, R., et al. 2020, arXiv e-prints, arXiv:2009.06537. <https://arxiv.org/abs/2009.06537>
- Schwadron, N., & McComas, D. 2021, arXiv preprint arXiv:2102.03696
- Shoda, M., Chandran, B. D., & Cranmer, S. R. 2021, arXiv preprint arXiv:2101.09529
- Squire, J., Chandran, B. D., & Meyrand, R. 2020, *Astrophys. J. Lett.*, 891, L2
- Squire, J., Quataert, E., & Schekochihin, A. 2016, *Astrophys. J. Lett.*, 830, L25
- Tenerani, A., & Velli, M. 2013, *J. Geophys. Res. Space Phys.*, 118, 7507
- Tenerani, A., Velli, M., Matteini, L., et al. 2020, *Astrophys. J. Suppl. Ser.*, 246, 32
- Van Ballegooijen, A., & Asgari-Targhi, M. 2016, *Astrophys. J.*, 821, 106
- van Ballegooijen, A. A., & Asgari-Targhi, M. 2017, *Astrophys. J.*, 835, 10
- Vasquez, B. J., & Hollweg, J. V. 1998, *J. Geophys. Res. Space Phys.*, 103, 335
- Velli, M., Grappin, R., & Mangeney, A. 1992, in *American Institute of Physics Conference Series*, Vol. 267, *Electromechanical Coupling of the Solar Atmosphere*, ed. D. S. Spicer & P. MacNeice, 154–159, doi: [10.1063/1.42861](https://doi.org/10.1063/1.42861)
- Verdini, A., & Velli, M. 2007, *Astrophys. J.*, 662, 669
- Wang, Y.-M., & Sheeley, N. 1990, *Astrophys. J.*, 355, 726
- Woodham, L., Horbury, T., Matteini, L., et al. 2020, arXiv preprint arXiv:2010.10379
- Zank, G., Nakanotani, M., Zhao, L.-L., Adhikari, L., & Kasper, J. 2020, *Astrophys. J.*, 903, 1